IDEA League

Master of Science in Applied Geophysics

Research Thesis

A clean convergent alternating projections onto convex sets method for data reconstruction

Miaoyang Yuan

August 2, 2024

A clean convergent alternating projections onto convex sets method for data reconstruction

Master of Science Thesis

for the degree of Master of Science in Applied Geophysics
by

Miaoyang Yuan

August 2, 2024

Department of Geoscience & Engineering
Department of Earth Sciences
Faculty of Georesources and Material Engineering

Delft University of Technology
ETH Zürich
RWTH Aachen University

IDEA LEAGUE
JOINT MASTER'S IN APPLIED GEOPHYSICS

Delft University of Technology, The Netherlands
ETH Zürich, Switzerland
RWTH Aachen, Germany

Dated: *August 2, 2024*

Supervisor(s):

Dr.ir. G.G. Drijkoningen

Dr.ir. D.J. (Eric) Verschuur

Dr. Yimin Sun

Committee Members:

Dr.ir. G.G. Drijkoningen

Dr.ir. D.J. (Eric) Verschuur

Dr. Yimin Sun

Dr. Ir. D.S. (Deyan) Draganov

Prof. Dr. sc. Florian M. Wagner

Abstract

Seismic data reconstruction addresses the challenge of accurately restoring incomplete or damaged seismic datasets, which is crucial for subsurface imaging and exploration. The missing data is often due to equipment failure, signal loss, environmental noise, or poor geological conditions. It may also result from limitations in data acquisition, such as sparse sampling and noise interference. This thesis proposes a Clean Convergent alternating Projections onto Convex Sets (CCP) method for data reconstruction. By incorporating an initial value tweaking step into the alternating projections process in the Convergent alternating Projections onto Convex Sets (CP) method, this method aims to reduce ringing noise in the reconstruction results by the CP method. Initially, the traditional CP method and its application in seismic data reconstruction are introduced, highlighting its shortcomings in addressing ringing noise. To overcome this issue, a CCP method based on a non-local means algorithm for initial value tweaking is proposed and applied within the outer loop of the CP method. The theoretical foundation and implementation steps of the CCP method are discussed in detail, and its effectiveness is validated through a series of experiments. The experimental results demonstrate that, compared to the traditional CP method, the CCP method significantly reduces ringing noise and improves the quality of the reconstructed data. Various datasets, including images, 2D seismic section data from the SEAM II Arid model, and 3D seismic model cubes, are used to showcase the reconstruction capabilities of the CCP method in different scenarios. Finally, the thesis provides an in-depth discussion of the CCP method, including intermediate results in the outer loop, the necessity of data preconditioning, and parameter testing, offering a practical set of control parameter settings. The study shows that the CCP method has broad application prospects in data reconstruction, providing valuable references for future research.

Acknowledgements

First of all, I would like to express my gratitude to all my colleagues and managers at Aramco Overseas Delft. Aramco Overseas Delft provided a genuine research environment and ample computational resources. It also allowed me to experience how a global research and development center operates.

In particular, I would like to thank my supervisor at Aramco Overseas Delft, Dr. Yimin Sun. He not only provided substantial academic support but, more importantly, taught me how to conduct research from scratch. I have learned to pay more attention to documenting my work and delving into the details of issues in my future work. I am deeply grateful for his guidance and dedication. I am also very grateful to Wenxiu Wang, who discussed various issues with me and shared her research experiences from her PhD journey in the edge computing group at Aramco Overseas Delft.

Additionally, I am very grateful to my two supervisors at TU Delft, Dr. ir. Guy Drijkoningen and Dr. ir. Eric Verschuur. They provided profound academic support and many invaluable suggestions. I also thank all the professors who taught me courses over the past two years. They helped me gain a deeper understanding of geophysics.

In particular, I am very grateful to the cohort of the IDEA League Applied Geophysics program. Here, I met partners from different countries, and we spent the past two years learning and exploring together. I especially want to thank Boyu Gao. We teamed up to complete many challenging projects and had many valuable discussions that extended beyond geophysics.

Finally, I am deeply grateful to my family. I thank my parents for their unwavering support, no matter how naive or capricious my ideas were. I also want to express my heartfelt thanks to all my friends who accompanied me, helping me to relax and recharge outside my research work. I would also like to thank Fyodor Dostoevsky and his novels, which filled my sleepless nights.

August 2, 2024

Thank you all from the bottom of my heart.

Delft University of Technology
August 2, 2024

Miaoyang Yuan

Chapter 1

Introduction

Effective reconstruction techniques aim to recover the missing data, thereby enabling more accurate interpretation of seismic information. In this chapter, we introduce the a seismic data reconstruction method under study, the Convergent Alternating Projections onto Convex Sets (CP) method, and its background. We will first explain the mathematical foundation of the Alternating Projections onto Convex Sets (POCS) method and present its reported applications in various fields. Then, we introduce the CP method, which enhances the AK-POCS method (a variant of the POCS method applied in the field of geophysics) by incorporating the Cauchy convergence criterion, making it more mathematically rigorous [22]. Finally, we identify an area where the CP method still requires improvement, which is the problem that this paper aims to address. The chapter concludes with an outline of the entire thesis.

1-1 POCS Method

Our introduction to the POCS method follows Sun and Quentin (2024)[22]. The POCS method is an iterative algorithm used primarily for solving under-determined problems where multiple constraints are present. Its primary objective is to find a point that lies within the intersection of several convex sets, which represent the constraints of the problem. In the POCS method, convex sets, projections and convergence condition are three key mathematical concepts[13]. Convex sets define the feasible region for solutions, acting as boundaries that the potential solutions must fall within. Projections are the mechanism through which an initial guess is refined step by step, towards the set that represents the problem constraints. The convergence condition is the criterion that ensures these iterative steps are productive, guiding the projections to ultimately converge to a point belonging to a common intersection of all convex sets, thus yielding a solution that fits all the prescribed constraints.

1-1-1 Convex sets

In mathematical terms, a set Ω is convex if for any two vectors $\vec{v_1} \in \Omega$ and $\vec{v_2} \in \Omega$, the relationship $\vec{v_1} + (1-\theta)\vec{v_2} \in \Omega$ holds for all $\theta \in [0,1]$[13]. A more accessible interpretation

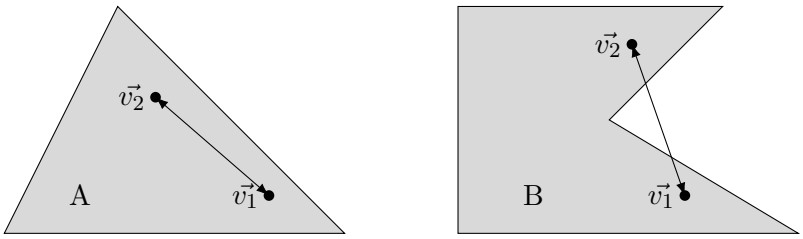

Figure 1-1: The set A is convex and the set B is non-convex.

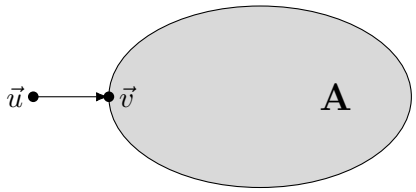

Figure 1-2: Projecting a vector $\vec{u}$ to the convex set A.

is that a set Ω is convex if the line segment connecting any two points in the set is fully contained in the set, as shown in Figure 1-1.

1-1-2 Projections

Geometrically, the meaning of projecting a vector onto a set is to find a vector within the set such that the distance between the two vectors is minimized[13], as shown in Figure 1-2. Mathematically, this projection operation is described as follows:

$$P(A) = argmin \mid\mid \vec{u} - \vec{v} \mid\mid, \quad \vec{v} \in A, \tag{1-1}$$

where $\vec{u}$ is a vector outside set A and $\vec{v}$ is a vector on the boundary of set A. The projection of $\vec{u}$ onto A is defined as finding the vector within A that is closest to $\vec{u}$. This projected vector is typically located on the boundary of A. However, in the special case where $\vec{u}$ already lies within A, the projection of $\vec{u}$ is $\vec{u}$ itself.

1-1-3 Projections onto convex sets

Based on the aforementioned definitions of convex sets and projection, we are able to elucidate the POCS algorithm. For the sake of clarity, we explain the algorithm using a simple scenario involving 2 or 3 convex sets, as shown in Figure 1-3 and 1-4. In the considered space, each point represents a specific data point. The collection of all points that fulfill a given constraint forms a convex set. In this context, projection is the computational method of mapping a point outside the convex set back onto it, thereby ensuring that the corresponding data point adheres to the constraint embodied by the convex set. Typically, the initial solution, which we aim to bring into compliance with the constraint, is outside these convex sets. Through iterative projections of this point onto multiple convex sets, it will eventually converge at the intersection of these sets, assuming they intersect. This convergence point is one viable solution, as illustrated in Figure 1-3.

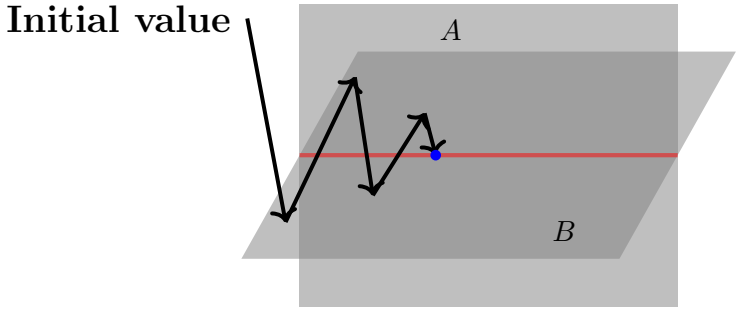

Figure 1-3: Graphical illustration of the POCS algorithm. The bright red line is the intersection between set A and set B. The black arrows represents the projection process.

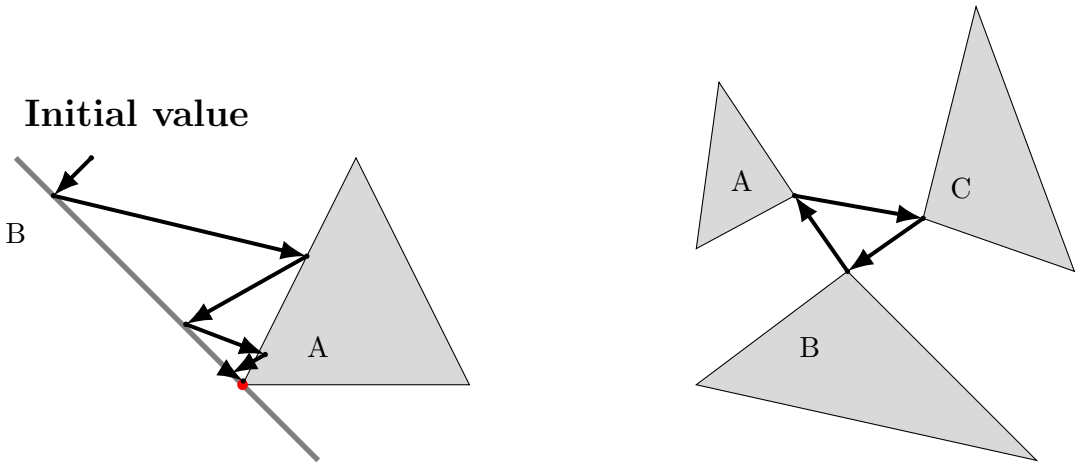

Figure 1-4: Two special cases for POCS: The intersection is only one point (left) and no intersection among convex sets (right).

1-2 Applications of POCS Method

POCS method was initially introduced by Bregman[3] and Gubin *et al.*[8] and was later popularized by Youla and Webb [26] and Sezan and Stark[19]. The POCS method was initially used for signal processing, particularly in reconstruction and restoration, which remains its most widely applied field. It has also seen successful applications in various other domains[13]. This section will introduce the diverse applications of the POCS method. In solving different problems, the concepts in the POCS method, such as convex sets, projections, and initial values, vary according to the specific application. In the final part, the application of the POCS method in geophysics for seismic data reconstruction will be discussed.

1-2-1 The Papoulis-Gerchberg algorithm in signal processing

The Papoulis-Gerchberg algorithm is a method to restore band-limited signals when only a portion of the signal is known[7][18]. This algorithm is one of the most classic applications of the POCS method. The two convex sets used in the Papoulis-Gerchberg algorithm are shown below:

$$A = \{u(x) \mid u(x) = i(x), \mid x \mid \leq X\}, \tag{1-2}$$

$$B = \{u(x) \mid U(\omega) = 0, for \mid \omega \mid > \Omega\}, \tag{1-3}$$

where $u(x)$ is a band-limit signal that only components in the band $\mid x \mid \leq X$ are known. $U(\omega)$ is the signal in the Fourier domain and Ω is the thresholding frequency in Fourier domain. The set A represents a known portion $i(x)$ of the signal when $\mid x \mid \leq X$. The set B is a low-pass band-pass filter in the Fourier domain. The procedure of the Papoulis—Gerchberg algorithm commences with an initial iteration from a known segment of the signal. Upon executing a Fourier transform on the signal, a projection onto set B is low-pass filtering the frequency components. The resultant signal is then projected onto set A to ensure consistency with the known signal. This iterative process is repeated until the outcome converges until the following condition is met,

$$\| o^{N+1}(x) - o^{N}(x) \| < \epsilon, \tag{1-4}$$

where $o^N(x)$ is the result after N iterations, and ϵ is a pre-defined residual level.

Clearly, signal restoration is an under-determined problem. Traditional methods, such as using polynomial extrapolation, only utilize a limited number of values. The Papoulis-Gerchberg method, on the other hand, ingeniously employs frequency domain low-pass constraints and known band-pass signal constraints to maximize the use of available information[13].

1-2-2 POCS method in source localization

Based on the previous application, the POCS method has become a method for solving under-determined problems and has been extended to various fields, such as signal deconvolution [16] and artificial neural networks[20]. However, the POCS method is not limited to

projections between just two sets; it can also involve projections among multiple sets, as long as these sets have a common intersection. The following application of the POCS method in the localization problem utilizes this idea.

Pinpointing an acoustic source using a sensor network, in a distributed manner and without the need to transmit the entire data set to a central processing unit, is the goal of localization[10]. Traditionally, this localization problem is tackled by nonlinear least-squares or maximum likelihood methods. However, these approaches often lead to complex global optimization challenges. The objective function in such cases may exhibit multiple local optima and saddle points, which can cause local search methods to converge to sub-optimal solutions. Although these methods can be asymptotically optimal under certain conditions, the presence of numerous local optima and saddle points can significantly hinder the efficiency and accuracy of the solution. The attenuation of acoustic waves can be modeled by:

$$y^l = \frac{A}{|| \, r^l - u \, ||^\beta}, \tag{1-5}$$

where A represents the source signal, r^l denotes the location of receiver l, u is the source location, β is the isotropic attenuation coefficient and y^l signifies the signal strength at receiver l. This equation assumes an idealized form of acoustic wave attenuation emanating from the source location u to receiver l. Based on Equation (1-5), we can build convex sets that constrain the source location u by disregarding the noise component and focusing on averaging the temporal variations:

$$D_l = \{u \in R^2 : || \, u - r^l \, || \leq [\frac{A}{y^l}]^{\frac{1}{\beta}}\}, \tag{1-6}$$

$$\hat{u} \in D = \bigcap_{L=1}^{L} D_L \subset R^2, \tag{1-7}$$

where $\hat{u}$ is location obtained by the POCS method, D_l is the location constraint modified by l, D is the intersection among D_l. This approach allows for the formulation of a simplified yet effective model to estimate the source location, leveraging the principles of convex optimization as embodied in the POCS algorithm. The projections of the POCS method are between a series of sets D_l.

Because there must exist a source, the series of sets D_L must intersect, which means that D exists. Projections onto the D sets can be carried out via the relaxation projection iterations:

$$u^{k+1} = u^k + \lambda_k [P_{D^l}(u^k) - u^k], \tag{1-8}$$

where λ_k is the relaxation parameter, which can accelerate the convergence speed. If $|| \, u - r^l \, || \leq [\frac{A}{y^l}]^{\frac{1}{\beta}}$, then $u \in D^l$, thus $P_{D^l} = 0$. In R^2 space, the projection is defined by Equation (1-9),

$$P_{D_l}(u^k) = r^l + [\alpha cos(\phi), \alpha sin(\phi)]^T, \tag{1-9}$$

where $\alpha = \sqrt{A/y^l}$, $\phi = atan(u^k(1) - r^l(1), u^k(2) - r^l(2))$. For a vector $x \in R^2$, $x(1)$ and $x(2)$ denote its first and second coordinates[10]. These iterations are repeated until reaching the

convergence criterion

$$|| \hat{u} - u ||< \epsilon, \tag{1-10}$$

where ϵ is a pre-defined residual level.

1-2-3 POCS in CT reconstruction

Computer Tomography (CT) scanning is essential in modern medical science, offering critical insights into internal structures. Enhancing image clarity and the signal-to-noise ratio during a CT scan is crucial. The POCS algorithm can significantly improve image resolution and clarity by iteratively refining the reconstruction process. This enhancement leads to more accurate diagnoses and treatment planning, highlighting the algorithm's versatility and effectiveness in complex medical imaging.

For divergent-beam CT, the source emits X-rays from a single point for each projection, with data captured by a 1D or 2D detector array. The following equation describes this physical process:

$$g_i = \sum_{j=1}^{M} A_{ij}\ u_j, \tag{1-11}$$

where A_{ij} is the system matrix element and is calculated by the intersection length of the ith ray through the jth pixel[12]. u_j is the image value of the jth pixel. The measurement g corresponds to the path integral of the X-ray attenuation coefficient across the source and detector bins. This integral is expressed as a weighted sum over the pixels transversed by the source-bin ray, given by equations (1-11).

A POCS-based scheme is adeptly designed to address problems involving constraints related to data fidelity and non-negativity, and is given by:

$$u^{n+1} = u^n + A_i \frac{g_i - A_i u^n}{A_i A_i^T}, \tag{1-12}$$

$$A :|| Au - g ||< \epsilon, \tag{1-13}$$

which define the data fidelity constraint mathematically. A POCS-like algorithm, also known as the Kaczmarz algorithm or the Algebraic Reconstruction Technique (ART), is embedded in the process of solving this linear system of equations. It represents the continuous projection onto the hyperplane formed by the ith row of the matrix A. This iterative process continues until Equation (1-13) is satisfied, where ϵ is a predefined residual target.

The non-negative constraint is defined as:

$$B : \{u(x) \mid u(x) = 0, for\ u(x) < 0\}. \tag{1-14}$$

With the convex sets A and B defined by Equation (1-13) through (1-14), a POCS method in CT reconstruction is constructed as:

1. Input the initial data $u_j^n = u_j^n$.
2. Iterative projections $u_j^{n+1} = u_j^n + A_i(g_i - A_i u_j^n)/A_i A_j^T$ until $|| Au - g ||< \epsilon$ (Set A).
3. $u_j = max\{u_j^{n+1}, 0\}$ (Set B).

In the POCS method, n is the iteration time and $n = 0$ represents the initial state.

1-3 Convergent POCS Method

1-3-1 AK-POCS in seismic data reconstruction

Many geophysicists have noted the flexibility and convenience of the POCS method. Seismic date reconstruction is a well-known under-determined problem in the geophysics society. Seismic data reconstruction is to recover missing or corrupted seismic data, which is crucial for accurate subsurface imaging and interpretation in geophysics and oil and gas exploration. The process involves using mathematical and computational techniques to fill in gaps in the seismic recordings, often caused by limitations in data acquisition. Methods such as prediction filter method, the sparse transform method, the rank reduction method and the nonlinear beamforming (NLBF) method[24] are used to estimate missing data based on known seismic signals and physical constraints[11].

In 2006, Amba and Kabir[1] proposed a seismic data reconstruction method based on the POCS method, and we refer to this method by AK-POCS. The concept of this method is similar to the Papoulis-Gerchberg algorithm, constructing two convex sets based on constraints in the Fourier domain and known information. Projections between these two convex sets yield the possible missing seismic data. Other geophysicists have used constraints in the curvelet domain[9] or radon domain[14], but AK-POCS is still widely used in the seismic industry due to its robustness and low computational cost.

To facilitate our discussion, we limit our mathematics in the 2D space although the generalization to a higher-dimensional space is straightforward. The AK-POCS method uses two convex sets shown below:

$$A = \{u(x,t) \mid u(x,t) = v(x,t), for\ known\ (x,t)\ locations,\ u, v \in R^2\}, \tag{1-15}$$

$$B_i \in B = \{u(k_x,f) \mid u(k_x,f) = 0, for\ known\ (k_x,f)\ locations,\ u \in C^2\}, \tag{1-16}$$

where $u(x,t)$ is the whole data set in the time domain, $v(x,t)$ is the known data set, $u(k_x,f)$ is the data set in $f-k_x$ domain.

Set A is defined to ensure that the data conform with the ground truth. The set B comprises a series of filters within the $f-k_x$ domain. The operations P_A and P_B describe the projection processes onto sets A and B respectively, and T representing a thresholding matrix.

$$P_A(u(x,t)) = \begin{cases} v(x,t), known\ location, \\ u(x,t), otherwise, \end{cases} \tag{1-17}$$

$$P_B(u(x,t)) = F_t^{-1} F_x^{-1} T F_x F_t u, \tag{1-18}$$

$$T(k_x, f) = \begin{cases} 1, if \mid \{F_x F_t u\}(k_x, f) \mid \geq p_k, p_k \in p, \\ 0, otherwise, \end{cases} \tag{1-19}$$

where F_x and F_t are the Fourier transform operators in time and spatial domain, F_x^{-1} and F_t^{-1} are the inverse Fourier transform operators in time and spatial domain. The p_k is a thresholding value in the set of threshold values p.

1-3-2 CP method

Comparing with the AK-POCS method, the CP method employs a rigorous convergence criterion before updating the convex set B_i,

$$|| \, u^{N+1}(x,t) - u^N(x,t) \, || < \epsilon \cdot || \, u^N(x,t) \, ||, \tag{1-20}$$

where ϵ represents the convergence ratio, $u^N(x,t)$ is the data set in time domain. In this method, during iterative mutual projections between sets A and B_i, B_i is updated only when the convergence between A and B_i has been reached. This approach renders the CP method a rigorous POCS method that can reach the algorithmic convergence eventually.

In the AK-POCS method, this convergence is hopefully achieved through a large number of iterations. Sun and Quentin[22] pointed out that AK-POCS is theoretical convergent under two conditions. First, the initial values of all the data set are zeros. Secondly, the thresholding value p_k is no larger than the maximum amplitude of result in $f - k_x$ domain after projecting onto set A. However, many of the projections might be unnecessary in AK-POCS. The CP method introduces an explicit convergence criterion, eliminating redundant computations and guaranteeing its mathematical convergence.

1-3-3 Examples of CP method

In this subsection, we demonstrate the CP method's ability to reconstruct missing data using three different application scenarios. Overall, the quality of the reconstruction results is acceptable, but we will point out one shortcoming of the CP method in the next subsection.

We present three types of data sets: synthetic linear seismic data, a 2D seismic section slice from the SEAM II Arid model, and a drill cuttings image. We set the same control parameters used in the CP reconstruction for all kinds of data. The maximum iteration number N is 10. The convergence ratio ϵ is 0.01. The reconstruction is implemented in the whole window. The thresholding function is defined as follow[6]:

$$p_k = p_{max} e^{b(m-1)}, \tag{1-21}$$

$$m = 1, 2, ..., N, \tag{1-22}$$

$$b = \frac{-1}{N-1} ln \frac{p_{max}}{p_{min}}, \tag{1-23}$$

where p_{max} and p_{min} are the maximum and minimum value of the sparse input in the $f - k_x$ domain, N is the maximum iteration number, which is 10 in our examples.

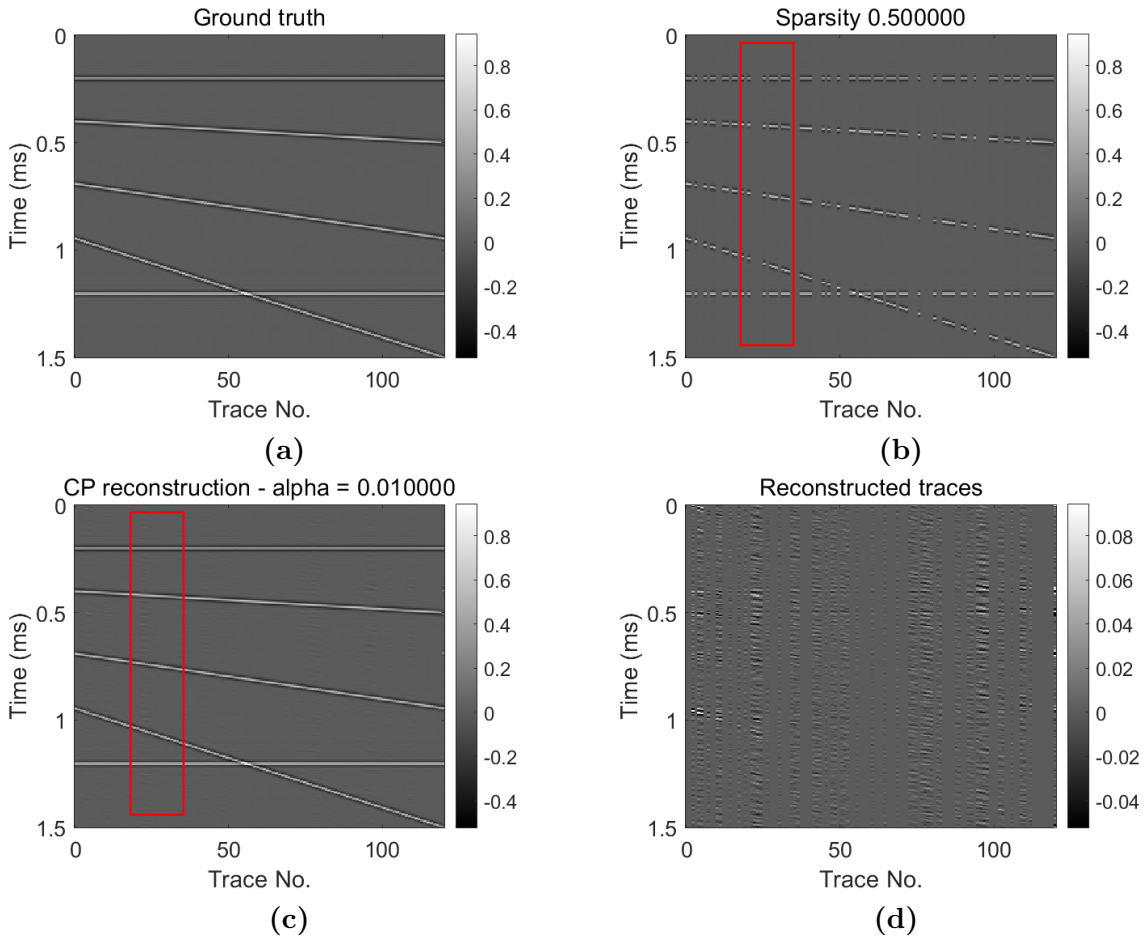

Figure 1-5: **(a)** Ground truth of the synthetic seismic data. **(b)** Sparse synthetic seismic data with 0.5 sparsity. **(c)** Reconstructed result by the CP method. **(d)** Difference between reconstructed seismic data and ground truth with plot gain.

Figure 1-5 shows the reconstructed result of a synthetic seismic data set with linear events. Figure 1-5a is the ground truth of the synthetic seismic data. Figure 1-5b is the sparse input data with 50% traces decimated randomly. Figure 1-5c is the reconstructed seismic data by the CP method. Figure 1-5d is difference between ground truth and CP reconstruction. To highlight the ringing noise, a plot gain of 10 times was used. The CP method performs well for the linear synthetic seismic data. The red boxes in Figure 1-5b and 1-5c highlight the reconstructed linear seismic events.

Figure 1-6 shows the reconstructed result for a 2D seismic section of a shot gather generated by the SEAM Arid Model. Figure 1-6a is the ground truth of this 2D section shot gather. Figure 1-6b is the sparse input with 30% decimated traces. Figure 1-6c is the reconstructed result by the CP method. Comparing with the ground truth, the reconstruction for this seismic 2D section in Figure 1-6 shows ringing noise. Ringing noise in Figure 1-6c such as highlighted in the red box reduces the quality of the CP reconstruction.

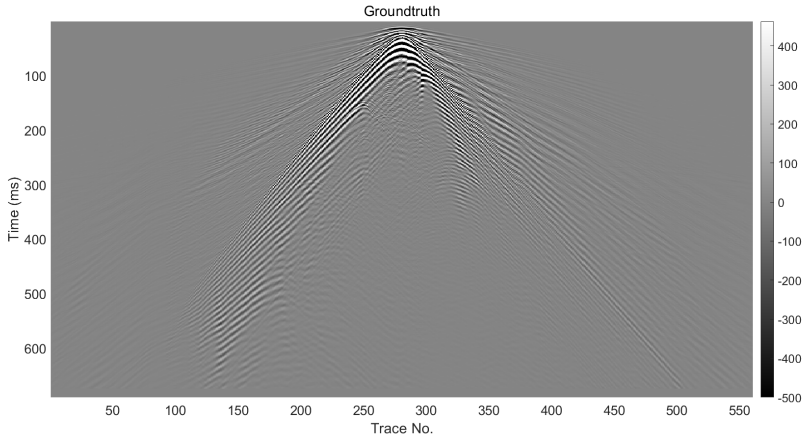

(a)

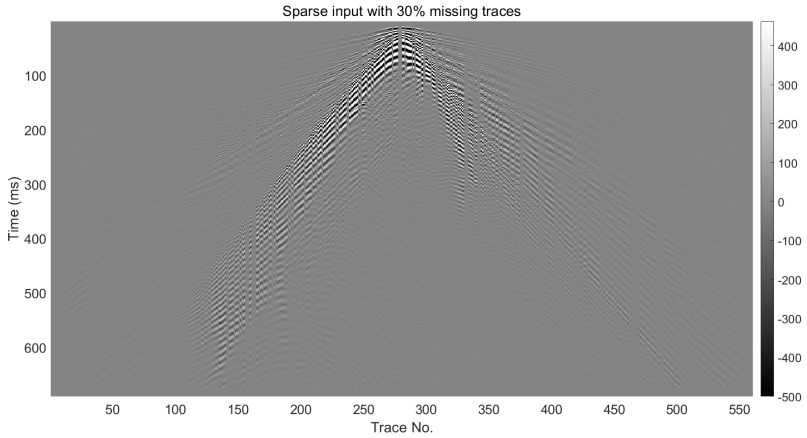

(b)

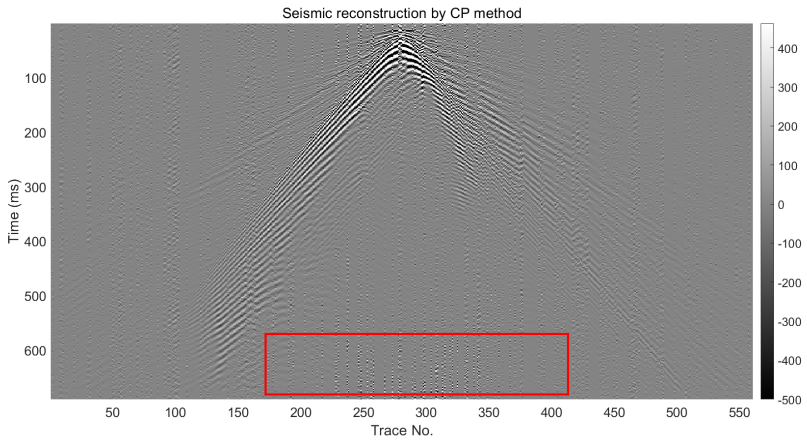

(c)

Figure 1-6: **(a)** Ground truth of a 2D seismic section. **(b)** Sparse 2D seismic section with 30% traces randomly decimated. **(c)** CP reconstruction section.

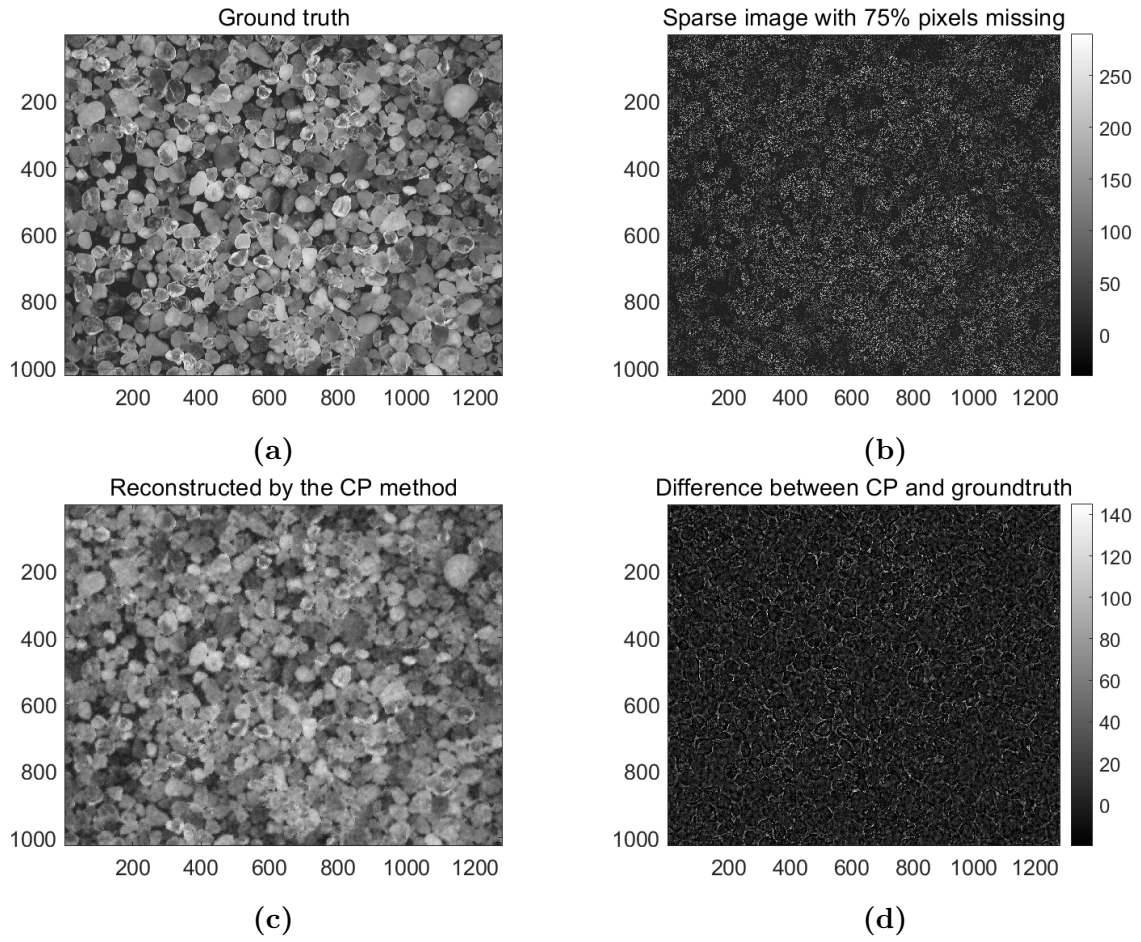

Figure 1-7: **(a)** Ground truth image. **(b)** Sparse image with 75% pixels missing. **(c)** econstructed image by the CP method. **(d)** Difference between reconstructed image and groundtruth image with plot gain.

Figure 1-7 shows the reconstructed result of a drill cuttings image[25]. Figure 1-7a is the ground truth of the drill cuttings image. Figure 1-7b is the sparse input with 75% pixels decimated. Figure 1-7c is the reconstructed image by the CP method. Figure 1-7d is the difference between Figure 1-7a and Figure 1-7c with 2x plot gain. The CP method also performs well in image reconstruction as it shown in Figure 1-7. This method can be extended to various types of data reconstruction problems. In addition to seismic data and image data, it can also be applied to the reconstruction of three-dimensional seismic model cubes[22].

1-3-4 Ringing noise

From the above three examples, we can observe that some reconstruction artifacts. For instance, in the reconstruction of the 2D seismic section of the SEAM Arid Model, the highlighted result in Figure 1-6c shows a significant amount of ringing noise, and Figure 1-5d and 1-7d illustrate the ringing noise with low amplitude.

The thresholding matrix is defined in equation (1-19). Its significance lies in the fact that after specifying the thresholding values p_k , all components in the $f - k_x$ domain that are above this magnitude are retained, while those below this magnitude are truncated. Regardless of the type of thresholding function we use to obtain our thresholding values, this truncation always exists. Such a hard thresholding scheme, in the frequency domain leads to the Gibbs phenomenon[21]. These Gibbs phenomena contaminate the final CP-reconstruction results, causing ringing noise and some local artifacts.

1-4 Thesis outline

In the following thesis, we present a new seismic data reconstruction method based on the CP method. Our method aims at suppressing ringing noise in CP-reconstructed results, and we refer to our method by the Clean Convergent POCS (CCP) method. The rest of the thesis is organized in the following manner:

- **Chapter 2: Theory of the Clean Convergent POCS (CCP) Method**
  In this chapter, we introduce the CCP method, including the idea of evolving from the CP method to the CCP method, and how this idea is implemented. The key component in the CCP method is an initial value tweaking operation based on the non-local means algorithm. Furthermore, data preconditioning schemes are introduced to deal with the different types of data.
- **Chapter 3: Examples**
  In this chapter, we present the results of the CCP method in different scenarios, including the reconstruction of 2D seismic data, image data, and 3D seismic model cubes. We will also provide a quality-evaluation metric to demonstrate the improvements of the CCP method over the CP method.
- **Chapter 4: Discussion**
  In this chapter, we delve into the details of the CCP method. This includes presenting the results of each outer loop iteration of the CCP method, comparing the direct implementation of the CCP non-local means algorithm on CP reconstructed results with those obtained from the CCP method, and examining the impact of preconditioning on the CCP method. Finally, we present comprehensive results of the parameter testing, and share our empirical guideline on setting control parameters in the CCP method.
- **Chapter 5: Conclusions**
  We wrap up our thesis with this chapter.

Chapter 2

Theory of Clean Convergent POCS (CCP) Method

In this chapter, we introduce the Clean Convergent POCS (CCP) method, which can yield high-quality data reconstruction results. Compared to the CP method, the CCP method incorporates an initial value tweaking step on top of alternating projections to supress ringing noise in data reconstruction. We introduce the initial value tweaking method, which uses a modified non-local means algorithm. It is important to note that the initial value tweaking method introduced in this thesis is not the only option for the CCP method, and we believe that more methods deserve further exploration.

2-1 Non-Unique Solutions in CP

Data reconstruction is a mathematically under-determined problem, meaning there exist non-unique solutions. When we use the CP method to solve this under-determined data reconstruction problem, we constrain the solution to the intersection of convex sets. Because the intersection in the solution space usually contains many points, the problem has many potential solutions.

2-2 Tweak initial values during the CCP process

From equation (1-1), it is evident that for a certain choice of the initial values, the result of alternating projections between defined convex sets is determined. The result obtained in the above CP method example is a point in the intersection of the convex sets as shown in Figure 2-1. In the CP method, the result containing ringing noise also belongs to the intersection of the convex sets. Our goal is to find a point (for example, the yellow point in Figure 2-1)

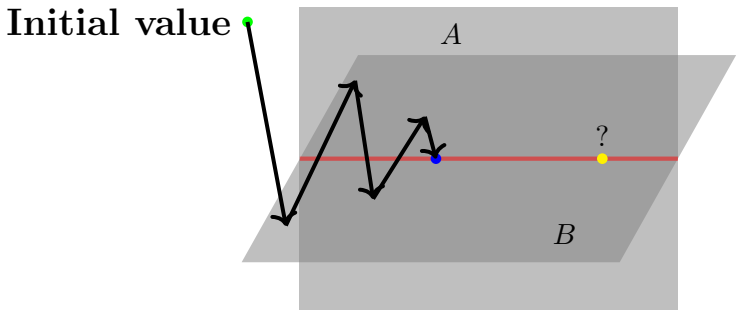

Figure 2-1: Graphical illustration of the POCS algorithm. The bright red line is the intersection between set A and set B. The black arrows represent the projections process. The blue dot represents the CP reconstruction result. The yellow dot represents a new reconstruction result with no or minimal ringing noise.

in this intersection that represents a data reconstruction result with no or minimal ringing noise.

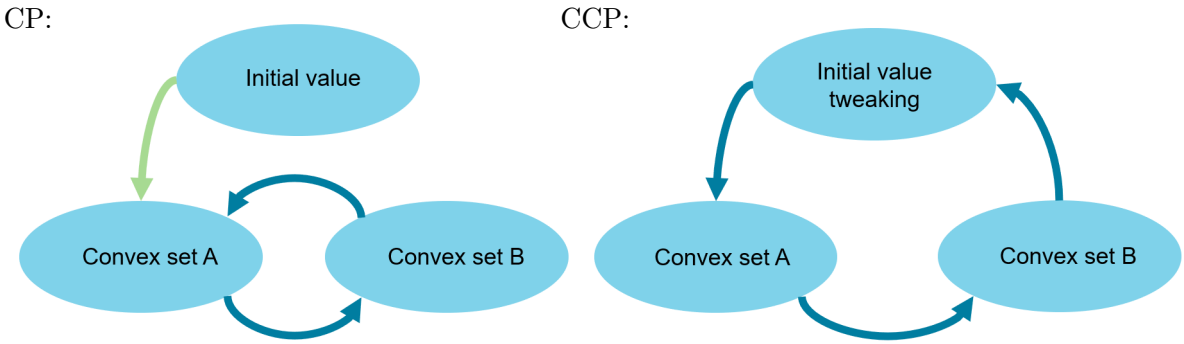

Figure 2-2: The differences between the CP and CCP concepts.

To achieve this, we need to add an additional step during the iterative projection process, tweaking the initial values. The initial values are the sparse input in the CP method. The mathematical concept is illustrated in Figure 2-2. Analogously, the CP method is like a mathematical free falling between two convex sets, whereas the CCP method with the initial value tweaking process is akin to a falling process under the influence of a guiding force. The geometrical illustration of the CCP method is shown in Figure 2-3

Using different initial value tweaking methods will result in the CCP method producing reconstructed results at different positions within the intersection. This is akin to applying forces in different directions in the solution space to alter the falling position. Since our goal is to suppress the ringing noise from the CP method's reconstruction results, we employ a technique similar to the non-local means filter to tweak the initial values in this thesis.

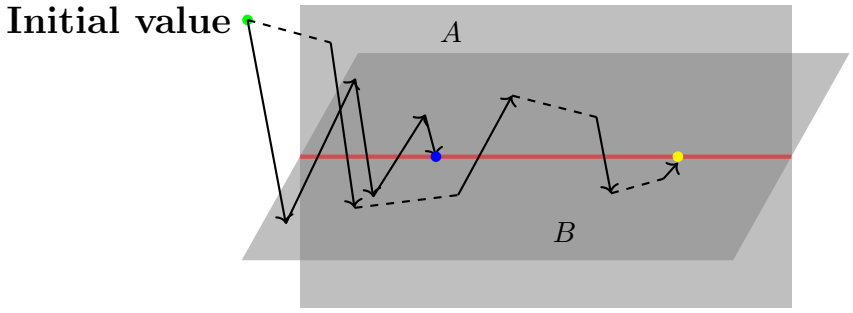

Figure 2-3: Geometric illustration of the CP and CCP method. Planes A and B represent two convex sets of constraints. The red line represents the intersection of the convex sets A and B, which is the solution set of this under-determined problem. The arrows represent the projection operations, and the dashed lines represent the initial value tweaking operations. The green dot indicates the initial value. The blue dot represents the solution obtained through the CP method. The yellow dot represents the solution obtained through the CCP method.

2-2-1 Non-local means method

In this subsection, we introduce the non-local means method[4], a denoising filtering method. Unlike other local smoothing filters, the non-local means filter does not limit its calculations to the neighborhood of a pixel but instead considers the entire local patch. This makes it more robust compared to the method of neighborhood filters[4].

Given the ith pixel $v(i)$ in the noisy image, the filtered pixel $M_{NL}[v](i)$ is defined as a weighted summation of all pixels in the search window I,

$$M_{NL}[v](i) = \sum_{j \in I} w(i,j)v(j), \tag{2-1}$$

where $w(i,j)$ is the weight matrix for the pixel j in the search window I. The pixel i is in the center of search window I in Figure 2-4. The weight matrix $w(i,j)$ is defined as,

$$w(i,j) = \frac{1}{Z(i)} e^{-\frac{||v(P_i)-v(P_j)||^2_{2,\alpha}}{h^2}}. \tag{2-2}$$

where h is a control parameter named filter sigma.$|| \, v(P_i) - v(P_j) \, ||^2_{2,\alpha}$ is defined as:

$$|| \, v(P_i) - v(P_j) \, ||^2_{2,\alpha} = G_\alpha * E \, || \, v(P_i) - v(P_j) \, ||^2_2, \tag{2-3}$$

where G_α is a Gaussian kernel with $\alpha > 0$ that refer to the spatial distance weight between i and j. $E \, || \quad ||$ is the Euclidean distance that represents the similarity between reference patch P_i and current patch P_j. As shown in Figure 2-4, the patch reference P_i is the blue box around pixel i and the current patch P_j is the gray box for every pixel $j \in I$. The normalizing constant $Z(i)$ is defined as:

$$Z(i) = \sum_{j \in I} e^{-\frac{||v(P_i)-v(P_j)||^2_{2,\alpha}}{h^2}}. \tag{2-4}$$

The non-local means filter not only require similarity between pixel i and pixel j but also demands that the points in the reference patch P_i around pixel i and the corresponding points in the current patch P_j around pixel j are similar. In Figure 2-4, the blue dots in the blue patch and the black dots in the gray patch represent points in the same relative positions. This requirement enhances the robustness of the method. Non-local means filtering has been successfully applied in various data reconstruction fields, such as emission tomography reconstruction[15] and CT reconstruction[5].

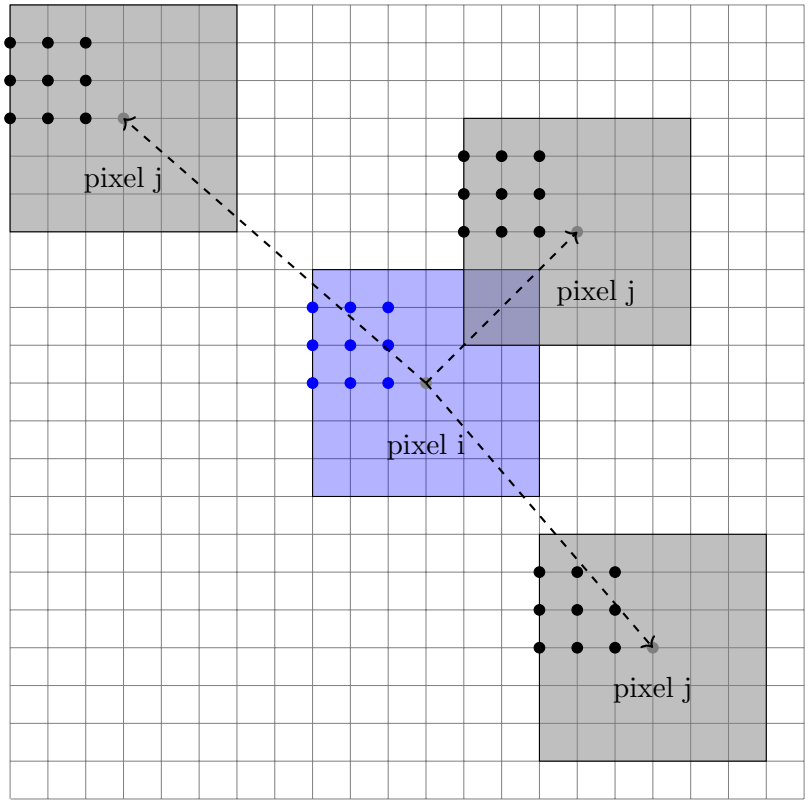

Figure 2-4: The diagram illustrates the non-local means filter. The entire grid represents the search window. The colored squares represent a pixel's non-local patch. The blue square represents the reference patch of the pixel i that needs to be processed. The gray squares represent the patches of other pixels j inside the search window. The black dots within the gray squares indicate the pixels that correspond to the same relative positions as the blue dots within the blue square.

2-2-2 CCP non-local means

In this subsection, we develop a CCP non-local means algorithm for the CCP method, which can be applied to various types of data, for instance, image data, 2D seismic data sections, and 3D seismic model cubes.

We apply our CCP non-local means algorithm during the data reconstruction process of the CCP method. In the initial iterations of alternating projections, there is a significant difference between the reconstructed result and the input data. If the unfinished

reconstruction results are used for non-local means filtering at this stage, the filter quality would be poor. Therefore, we only use the input sparse data, which includes ground truth information, to calculate the CCP non-local means, rather than using all the reconstructed data. Kindly note that this is the key feature of our CCP non-local means algorithm.

This modification introduces a distinction between this algorithm and the non-local means algorithm. For different j data point, the number of data points involved in calculating the weight may vary when the reference patch matches different current patches as illustrated in Figure 2-5. Therefore, we need to add a normalization factor in our CCP non-local means algorithm, which is mathematically described as:

$$w(i,j) = \frac{1}{Z(i)} e^{-\frac{||\delta(P_i,P_j)\cdot[v(P_i)-v(P_j)]||^2_{2,\alpha}}{n(\delta)\cdot h^2}}, \tag{2-5}$$

$$Z(i) = \sum_{j \in I} e^{-\frac{||\delta(P_i,P_j)\cdot[v(P_i)-v(P_j)]||^2_{2,\alpha}}{n(\delta)\cdot h^2}}, \tag{2-6}$$

where $n(\delta)$ is the number of data points matched between the reference patch P_i and the current patch P_j, and $\delta(P_i, P_j)$ is 1 if a point exists both in P_i and P_j and 0 otherwise. This step ensures that the weight $w(i,j)$ calculated for different matching patches does not change significantly due to the number of matched data points.

Figure 2-5 is an illustration of the CCP non-local means algorithm in image reconstruction. The entire grid represents the search window. The white dots are the missing data points in the sparse input data. As represented by $\delta(P_i, P_j)$, the data points used to calculate the CCP non-local means weights are not every one in the patch but only those that meet the following two conditions: 1) The data points in the reference patch P_i exist in the sparse input, and the reconstructed data point i is considered as ground truth in reference patch P_i. 2) The data points in the current patch P_j which have the same relative positions as these points casidered in P_i. In the Figure 2-5, the red highlighted pixels in current patches (gray boxes) meet the above requirements.

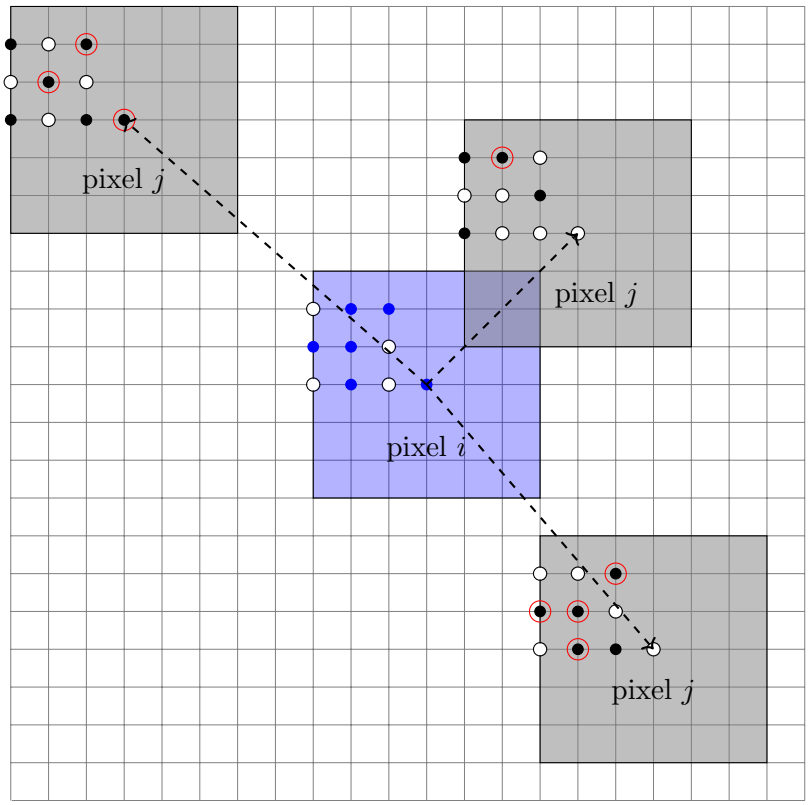

Figure 2-5: The diagram illustrates the CCP non-local means algorithm for image data. The entire grid represents the search window. The colored squares represent a pixel's non-local patch. The blue square represents the reference patch of the pixel i that needs to be processed. The gray squares represent the patches of other pixels j inside the search window. The black dots within the gray squares indicate the pixels that correspond to the same relative positions as the blue dot within the blue square. The white dots are the missing pixels in the sparse input data. The highlighted (red) dots are the pixels matched in our algorithm, representing those data points in $\delta(P_i, P_j)$ that bear the value of 1. The number of matched pixels for each current patch is $n(\delta)$.

Next, we extend this CCP non-local means algorithm to 2D seismic data as shown in Figure 2-6. Compared to image data, 2D seismic data differs in that each column represents a trace. Using patches that contain only one column allows for a better comparison of similarity between traces, adhering to the physical principles of 2D seismic data where the columns refer to traces. The number of matched data points $n(\delta)$ is the same for each patch and is related to the size of each patch. The dark gray patches represent the existent data in the sparse input. The shallow gray patches represent the missing data in the sparse input, which is then ignored in the CCP non-local means algorithm.

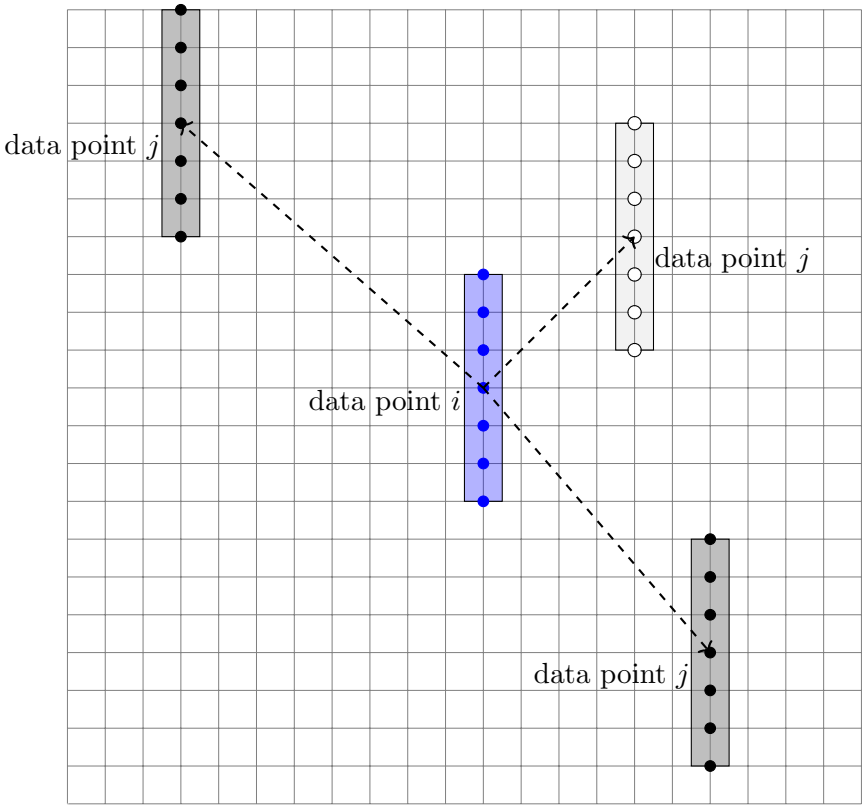

Figure 2-6: The diagram illustrates the CCP non-local means for 2D seismic data. The entire grid represents the search window. The small columns represent a data point's non-local patch. The blue column is the reference patch of the data point i that needs to be processed. The gray columns represent the patches of other data points j inside the search window. The black dots within the dark gray patch indicate this column is an existing trace. The white dots within the shallow gray patch indicate this column is a missing trace.

For 3D seismic model cubes, the CCP non-local means algorithm is demonstrated in Figure 2-7. The number of matched data points $n(\delta)$ follows the same rule as the case in 2D seismic section reconstruction if the seismic model misses data points in the z or time direction completely. By comparing the Euclidean distance between different traces, we calculate the similarity between different data points, aiming to achieve a more robust reconstruction result.

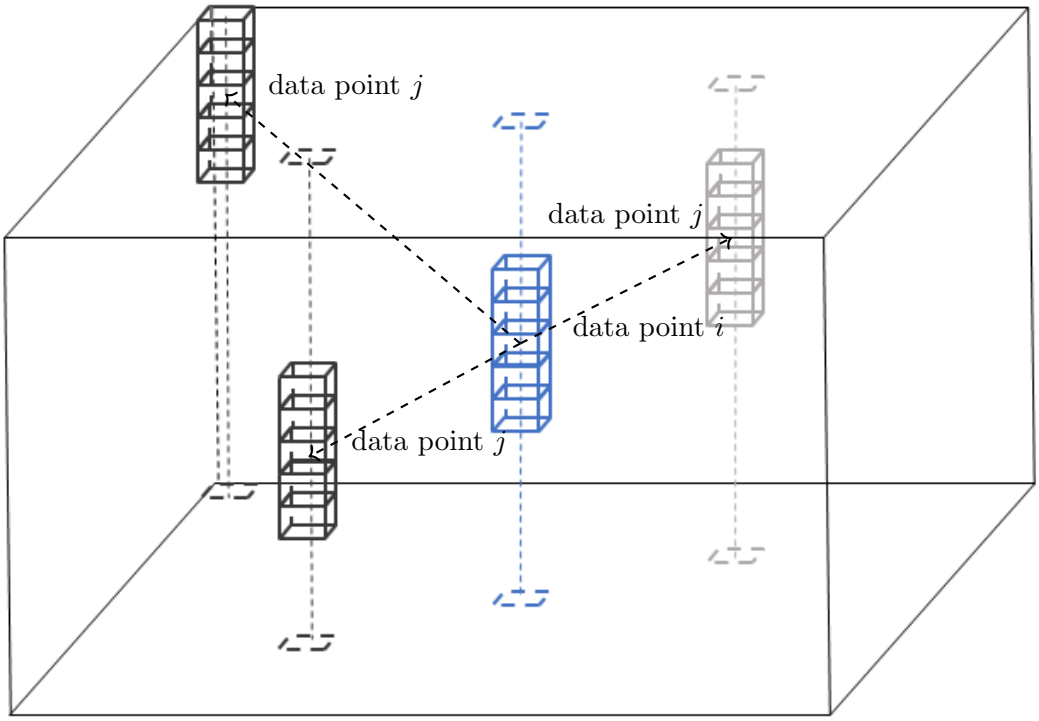

Figure 2-7: The diagram illustrates the CCP non-local means algorithm for a 3D seismic model cube. The entire cube represents the search window. The blue column is the reference patch of the data point i that needs to be processed. The gray columns represent the patches of other data points j inside the search window. The dark gray patch is located in an existing column in the sparse input. The shallow gray patch is located in a missing column in the sparse input.

2-2-3 Preconditioning

When we use the CCP method to reconstruct different types of data, the numerical range of the data vary. In cases where the dynamic range of the numerical value of data is extremely large, weights $w(i,j)$ may become so small that they are effectively ignored (approaching zero), rendering the CCP non-local means algorithm ineffective. Table 2-1 shows the ranges for different types of data.

The non-local means algorithm is often used for processing images with a dynamic range of 0 to 255. However, for 2D seismic data with a very large dynamic range and 3D seismic model cubes with a very small dynamic range, we need to precondition the data for our CCP non-local means algorithm. We present two ways to precondition input data, a linear

Table 2-1: Dynamic ranges for different types of data used in this thesis.

Data Type	Max	Min
2D SEAM Arid II Data	1.1570×10^4	-1.2507×10^4
Image Data	255	0
3D Seismic Model	9.6000×10^{-5}	-9.6000×10^{-5}

preconditioning way and a logarithmic one.

The linear preconditioning is descibed as:

$$f(u) = \frac{u(x) - min[u(x)]}{max[u(x)] - min[u(x)]}, \tag{2-7}$$

$$u(x) = f^{-1}(u) = min[u(x)] + f(u) \cdot (max[u(x)] - min[u(x)]), \tag{2-8}$$

where $u(x)$ is the data value, $min[u(x)]$ and $max[u(x)]$ are the minimum and maximum of the data value, and $f(u)$ is the result after linear preconditioning. Equation (2-8) represents the inverse process of this linear preconditioning.

The logarithmic preconditioning is described as follows:

$$f(u) = \begin{cases} -ln(1 - u(x)), & u(x) < 0 \\ 1n(1 + u(x)), & u(x) \geq 0 \end{cases} \tag{2-9}$$

$$u(x) = f^{-1}(u) = \begin{cases} 1 - e^{f(u)}, & u(x) < 0 \\ e^{f(u)} - 1, & u(x) \geq 0 \end{cases} \tag{2-10}$$

where $u(x)$ is the data value, and $f(u)$ is the result after logarithmic preconditioning. The linear preconditioning is utilized in the 3D seismic model cube and the logarithmic preconditioning is utilized in 2D SEAM Arid II data. Note that we can choose whether or not to precondition the input data based on the input data type. The preconditioned results of Table 2-1 is shown in Table 2-2.

Table 2-2: Dynamic range after preconditioning.

Alter preconditioning	Max	Min
2D SEAM Arid II Data	9.3563	−9.4341
Image Data	255	0
3D Seismic Model	1	0

2-3 CCP method

Based on the content introduced earlier in this chapter, the complete flowchart of the CCP method is presented in Figure 2-8b. Compared to the flowchart of the CP method in Figure 2-8a, the CCP method includes an additional initial value tweaking step in the data domain within the outer loop. The initial value tweaking step has the following key operations

- **Optional data preconditioning:** For data with different dynamic ranges, an appropriate preconditioning can be applied to achieve a reasonable dynamic range for CCP non-local means method to work properly.
- **CCP non-local means algorithm:** The CCP non-local means algorithm calculates the weight matrix $w(i)$ by comparing the similarity between the existing data (partial ground truth) in the input data and the reconstructed data in non-local patches, and use these weights to tweak the initial values.

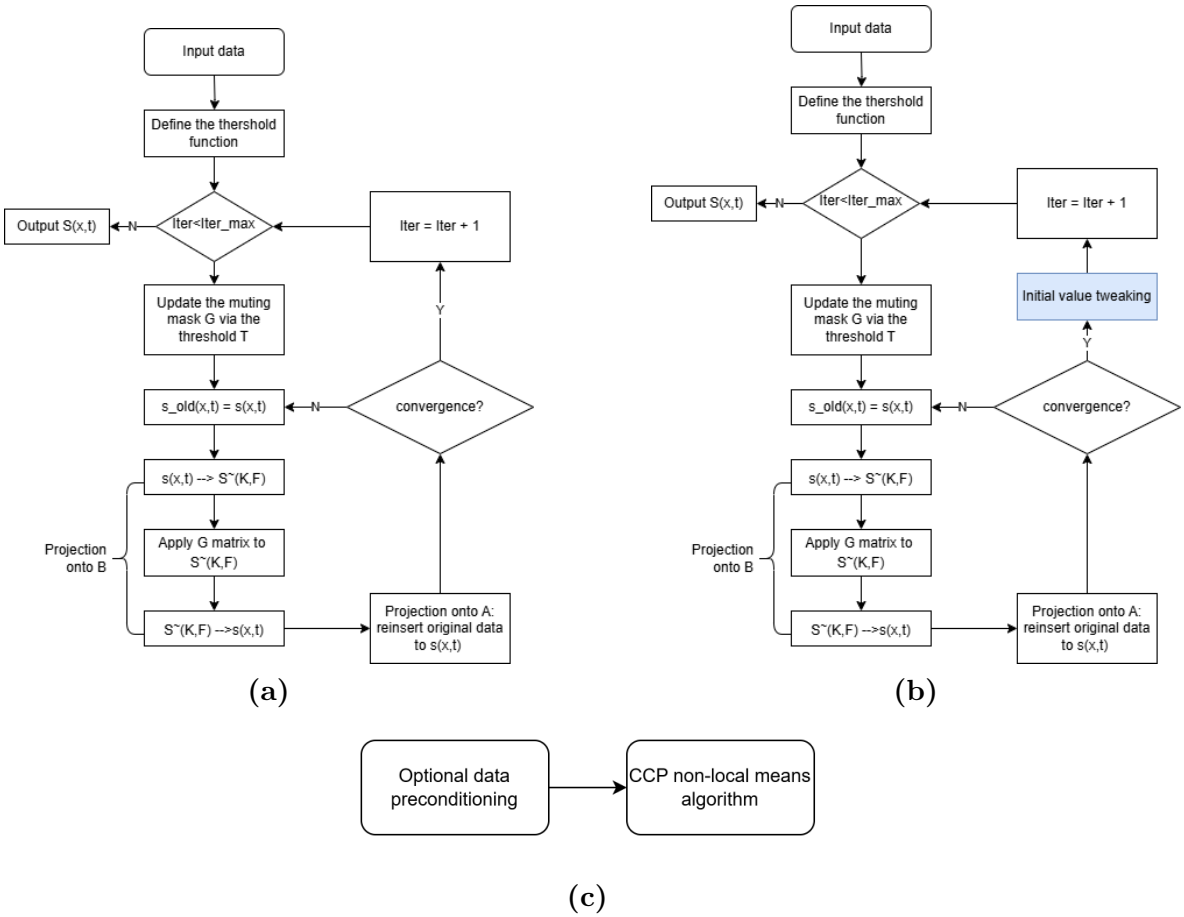

Figure 2-8: **(a)** Flowchart of the CP method. **(b)** Flowchart of the CCP method. An initial value tweaking step is added. **(c)** Flowchart of the initial value tweaking step.

Chapter 3

Examples

In the following chapter, we present the reconstruction results of the CCP method in various data sets, including images, 2D seismic section and 3D seismic model cubes. By comparing the reconstruction results with those of the CP method, the CCP method's capability on suppressing ringing noise and improving the result quality is well demonstrated.

3-1 Metric of reconstruction quality

Generally speaking, it is common choice to use the signal-to-noise ratio (SNR) of the reconstruction results based on the ground truth as the metric function. However, a single numerical value may not adequately reflect the quality of high-dimentional reconstruction results, for instance, 1D traces, 2D images and 3D data. Therefore, we design a statistical metric function to reflect the quality of high-dimensional reconstruction results. The metric function is defined as:

$$Error(i) = \frac{\mid D_{recon}(i) - D_{gt}(i) \mid}{\mid D_{gt}(i) \mid}, \tag{3-1}$$

where $D_{recon}(i)$ is the value of reconstructed element i, $D_{gt}(i)$ is the value of ground truth element i. $Error(i)$ is the error of the reconstructed element i. The results quality can be measured by analyzing the histogram of $Error(i)$ and evaluating the mean of $Error(i)$, which is defined as $\frac{1}{n}\sum Error(i)$.

3-2 Control parameters

The common control parameters for the CP and CCP methods include maximum iteration number N being 10, convergence ratio ϵ being 0.01, and the thresholding function defined as equations (1-21) through (1-23). The additional control parameters in the CCP method vary depending on the data type listed in the table 3-1. Comprehensive parameter testing results

will be shown in Chapter 4.

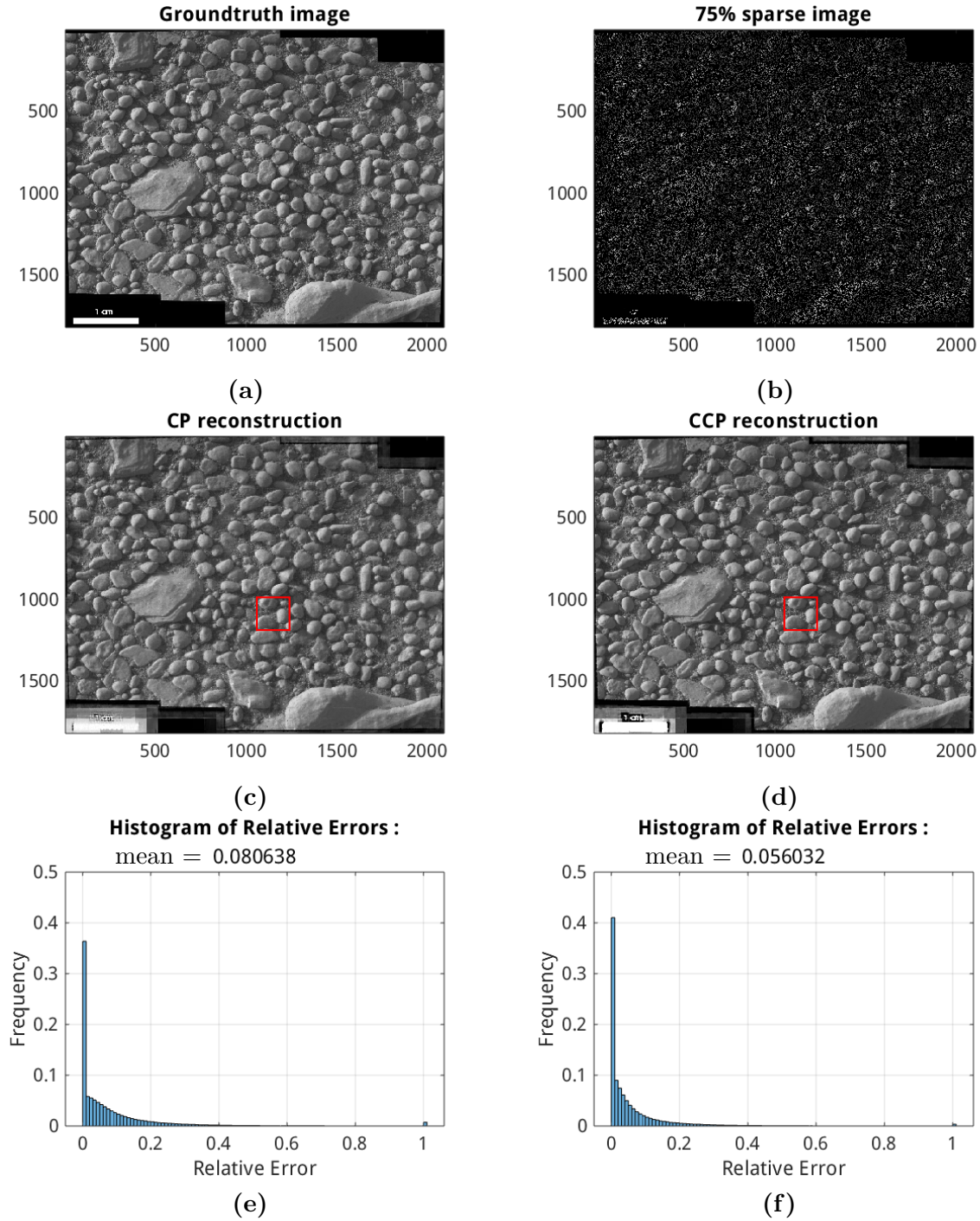

Figure 3-1: **(a)** Ground truth of the Mars desert image. **(b)** Sparse data with 75% pixels missing. **(c)** Reconstructed image by the CP method. **(d)** Reconstructed image by the CCP method. **(e)** Quality metric for (c). **(f)** Quality metric for (d).

Table 3-1: Control parameters of the CCP method for the examples in this chapter.

Data	Patch Size	Window Size	α	h	Windowing Size	Moving step
Image Data	9*9	15*15	4	10	128*128	64
2D Seismic	15*1	19*19	0.25	0.10	128*128	32
3D Model	5*1*1	9*9*9	0.20	0.10	64*41*40	16

3-3 Images

We first use the CCP method for reconstructing images. Both the CP and the CCP method use a reconstruction window of 128 pixels by 128 pixels, and the window moving step is 64 in both directions. Figures 3-1a and 3-3a show the ground truth images, with Figure 3-1a depicting a Mars desert scene and Figure 3-3a showing drill cuttings [25]. Figures 3-1b and 3-3b show the sparse input of each original image with 75% randomly decimated pixels. Figures 3-1c, 3-1d, 3-3c, 3-3d show the reconstructed images by the CP method and the CCP method. Figures 3-1e, 3-1f, 3-3e, 3-3f are the histograms of the quality metric function for each method with the mean of every relative errors of each element. Figures 3-2 and 3-4 present the reconstructed result in the highlighted window on Figures 3-1 and 3-3, indicating that the CCP method suppresses the ringing noise.

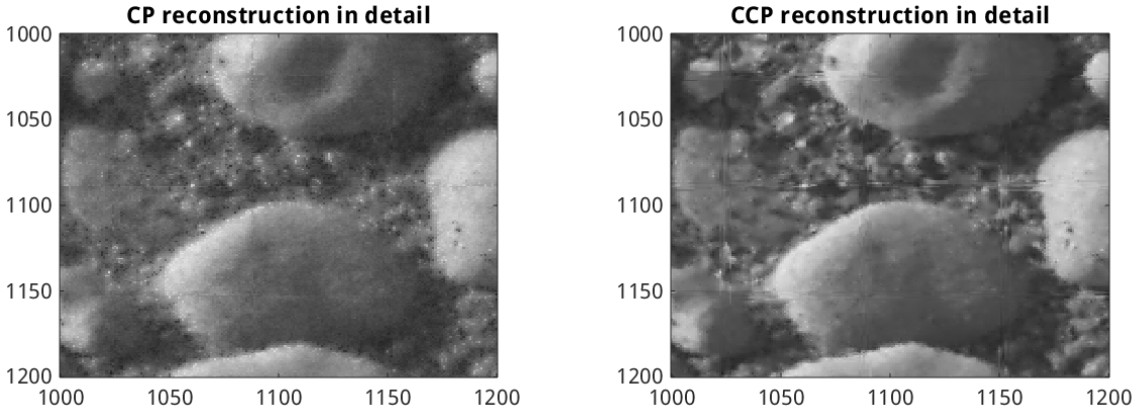

(a) **(b)**

Figure 3-2: **(a)** Detail of reconstructed Mars desert image by the CP method highlighted in Figure 3-1c. **(b)** Detail of reconstructed Mars image by the CCP method highlighted in Figure 3-1d.

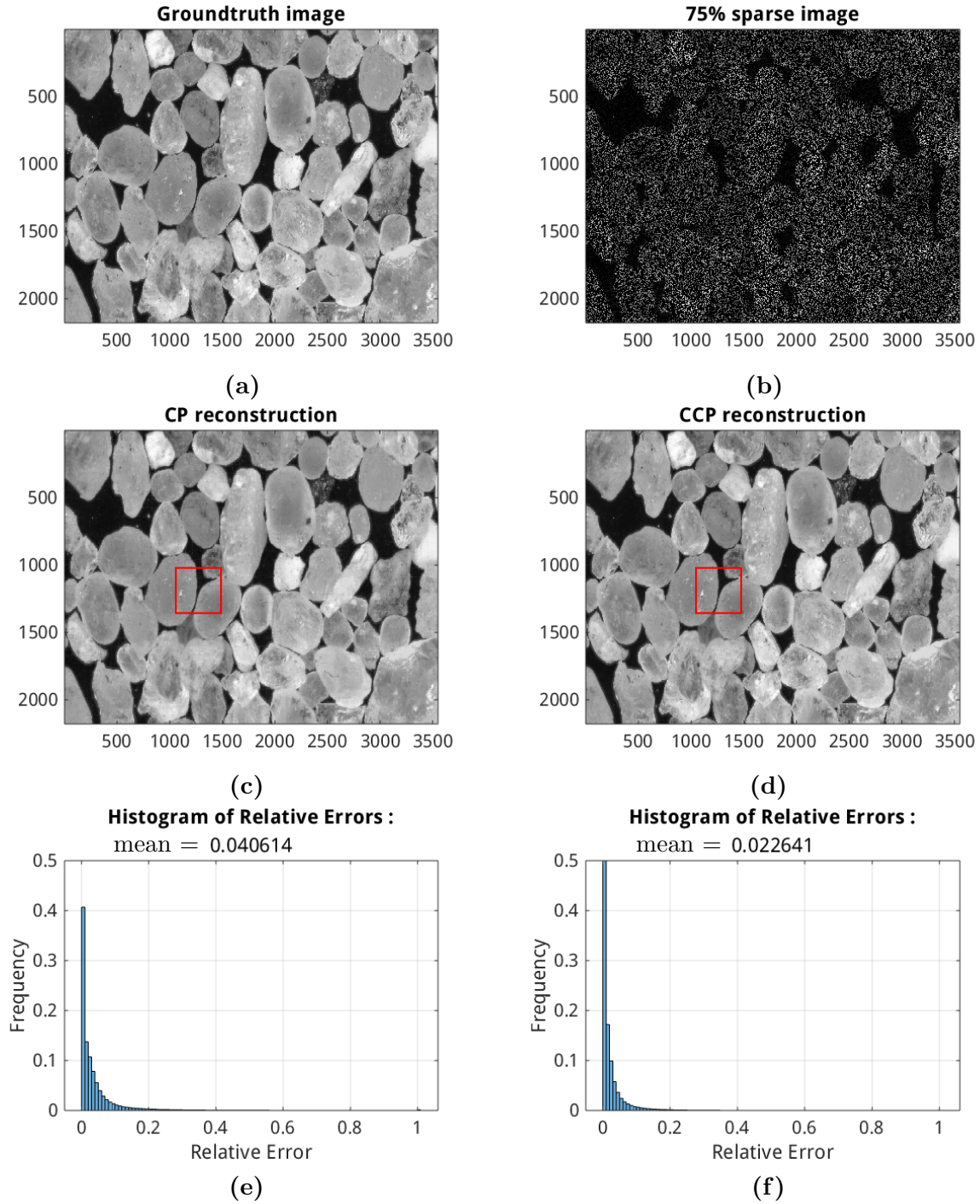

Figure 3-3: **(a)** Ground truth of the drill cuttings image. **(b)** Sparse data with 75% pixels missing. **(c)** Reconstructed image by the CP method. **(d)** Reconstructed image by the CCP method. **(e)** Quality metric for (c). **(f)** Quality metric for (d).

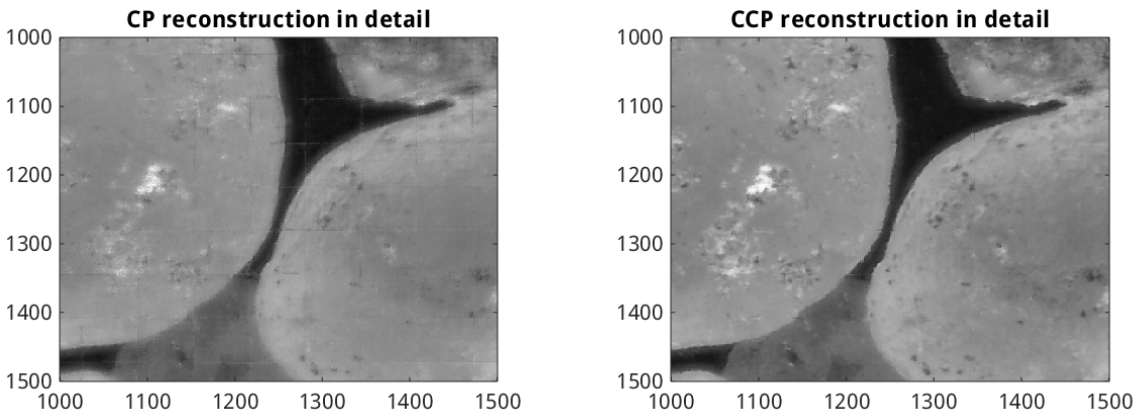

(a) (b)

Figure 3-4: **(a)** Detail of reconstructed drill cuttings image by the CP method highlighted in Figure 3-3c. **(b)** Detail of reconstructed drill cuttings image by the CCP method highlighted in Figure 3-3d.

3-4 2D seismic section reconstruction

3-4-1 SEAM Arid model

The SEAM (SEG Advance Modeling) Arid model is a sub-project within the SEAM project by SEG, utilizing the finite difference method to simulate seismic data for arid regions. The 2D section of the SEAM Arid V_p model[17] is shown in Figure 3-5. We use several 2D sections of a SEAM Arid shot gather to test the reconstruction capability of the CCP method: a 2D seismic section from the middle of this shot gather and another section at one end.

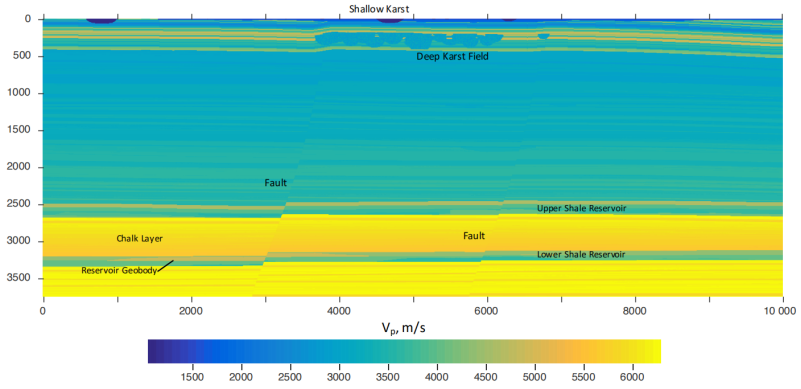

Figure 3-5: A 2D section of the 3D SEAM Arid V_p model.

3-4-2 Results

The reconstruction results of the 2D seismic section using the CP and CCP methods are shown in Figures 3-6 to 3-11. Figures 3-6a and 3-9a are the ground truth of 2D

seismic section NO. 270 and NO. 200. Section NO. 270 is near the middle of this shot gather and section NO. 200 is close to the end. The sparse input with 30% randomly decimated traces are shown in Figure 3-6b and 3-9b. The CP reconstruction results and CCP reconstruction results are shown in Figure 3-7a 3-7b, 3-10a and 3-10b. The red highlighted area in each figure reflect the suppression of ringing noise. Figure 3-8 and 3-11 show the reconstruction quality measured by the metric function we mentioned above. Note that. Both the CP and CCP reconstruction use a reconstruction window with 128 by 128 data points and a moving step of 32 data points in both vertical and horizontal directions.

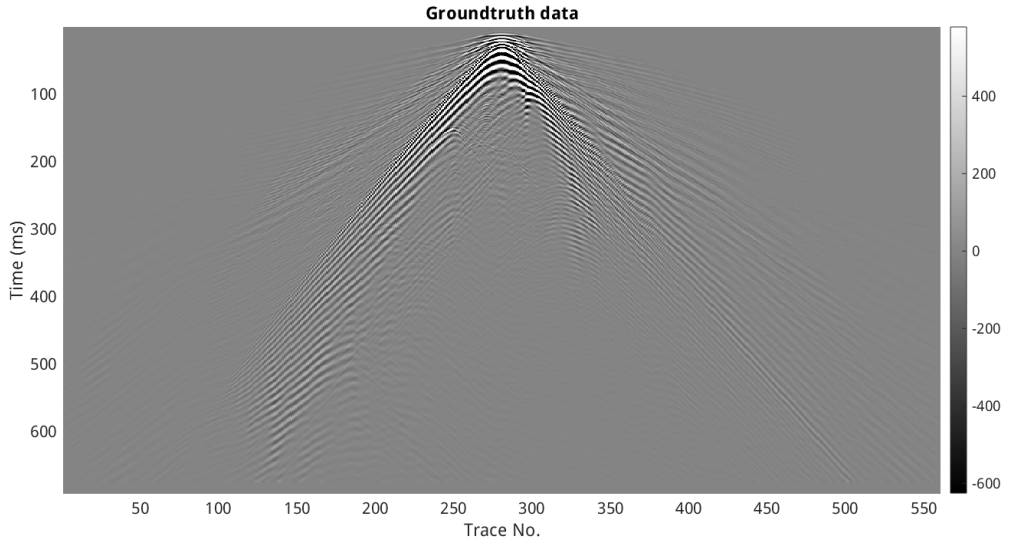

(a)

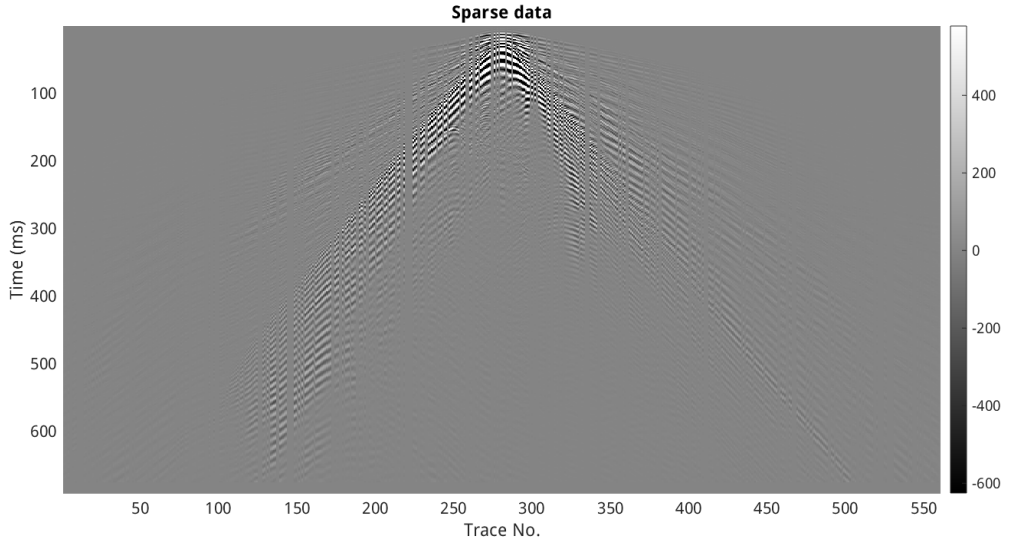

(b)

Figure 3-6: **(a)** Ground truth of the 2D section NO. 270 **(b)** Sparse input with 30% randomly decimated traces.

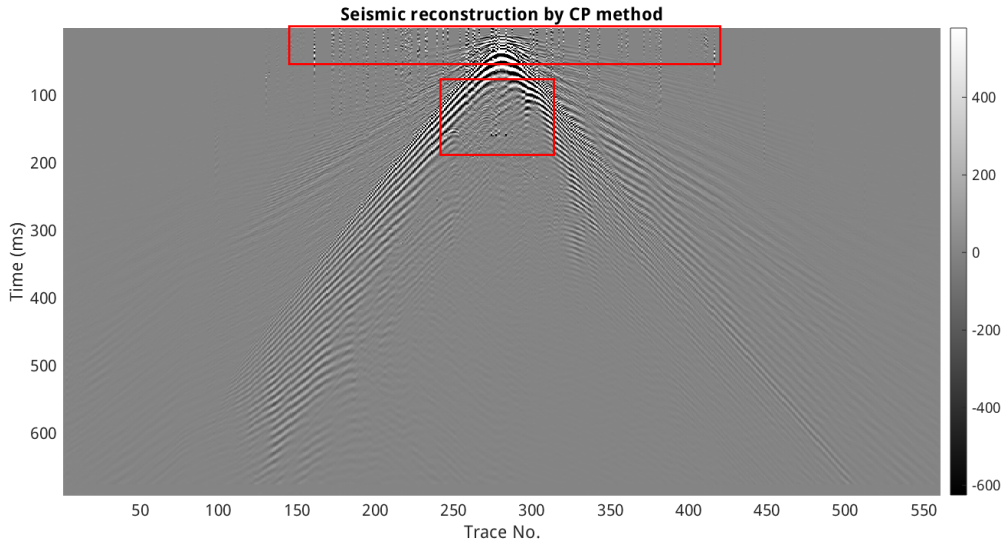

(a)

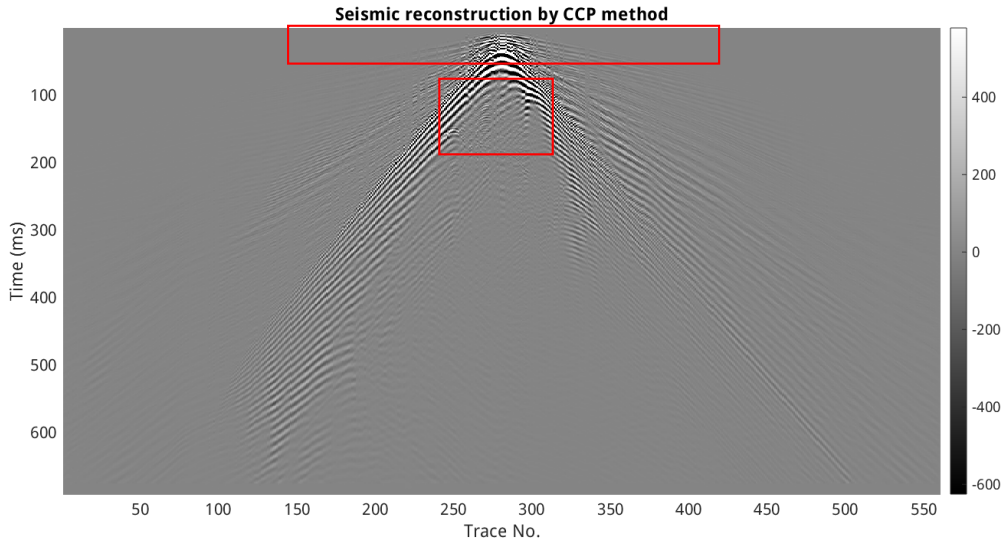

(b)

Figure 3-7: The reconstructed 2D seismic section NO. 270 using **(a)** the CP method and **(b)** the CCP method.

(a) (b)

Figure 3-8: Histogram of the metric function for **(a)** Figure 3-7a and **(b)** 3-7b.

It is important to note that some reconstructed elements are more than twice the original ground truth values, resulting in relative errors larger than 1. In the metric function, to ensure that different histograms have the same x-axis, all relative errors greater than 1 are displayed as 1 on the histogram. However, when calculating the mean, values greater than 1 are still used.

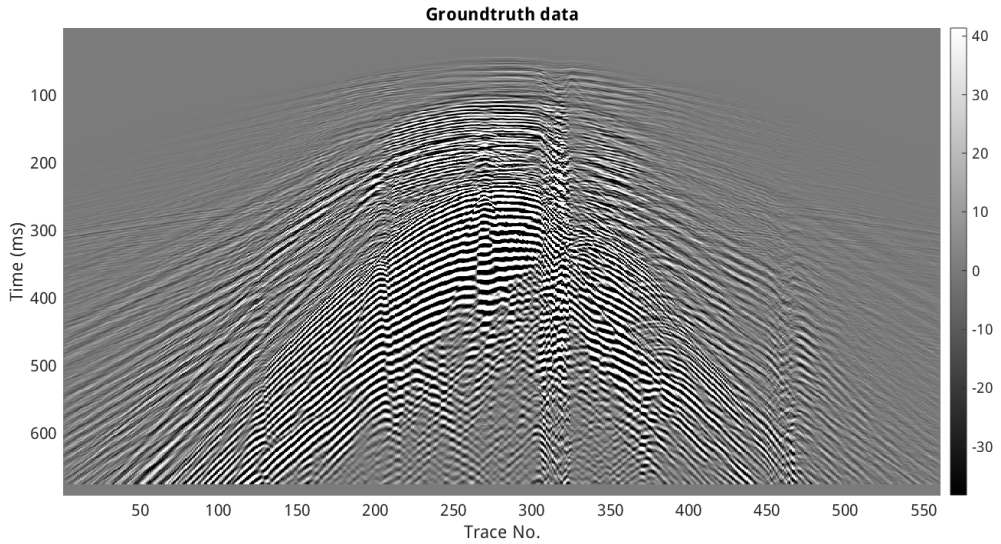

(a)

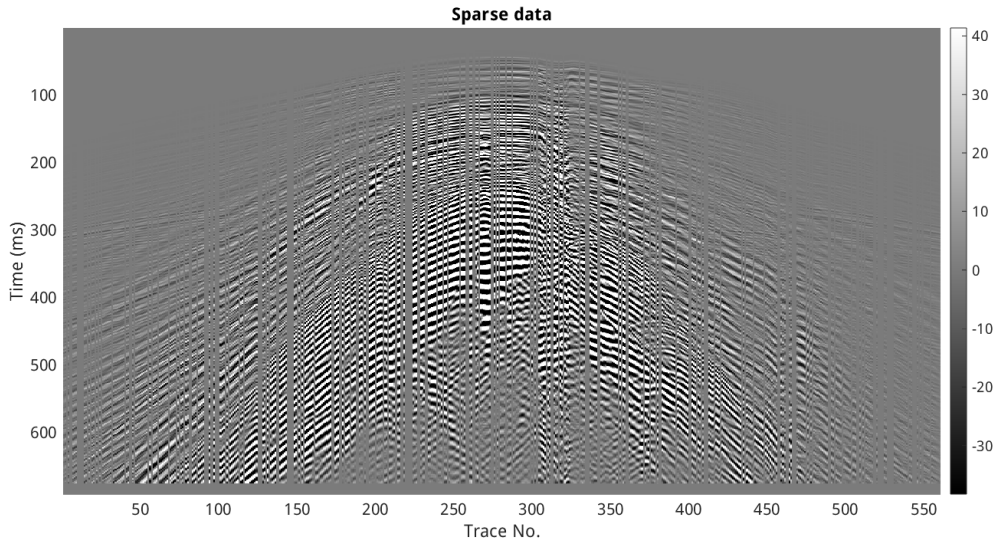

(b)

Figure 3-9: **(a)** Ground truth of the 2D section NO. 200 **(b)** Sparse input with 30% randomly decimated traces.

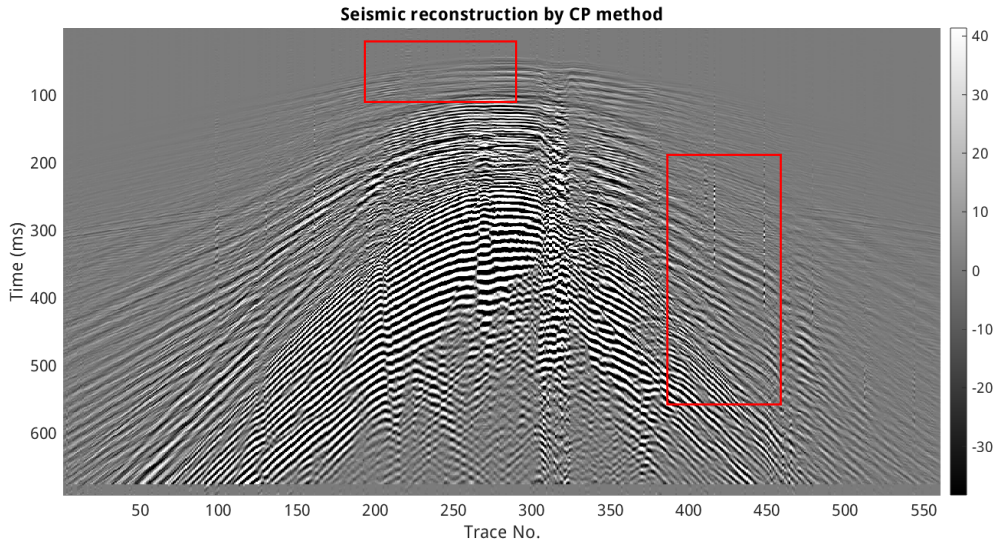

(a)

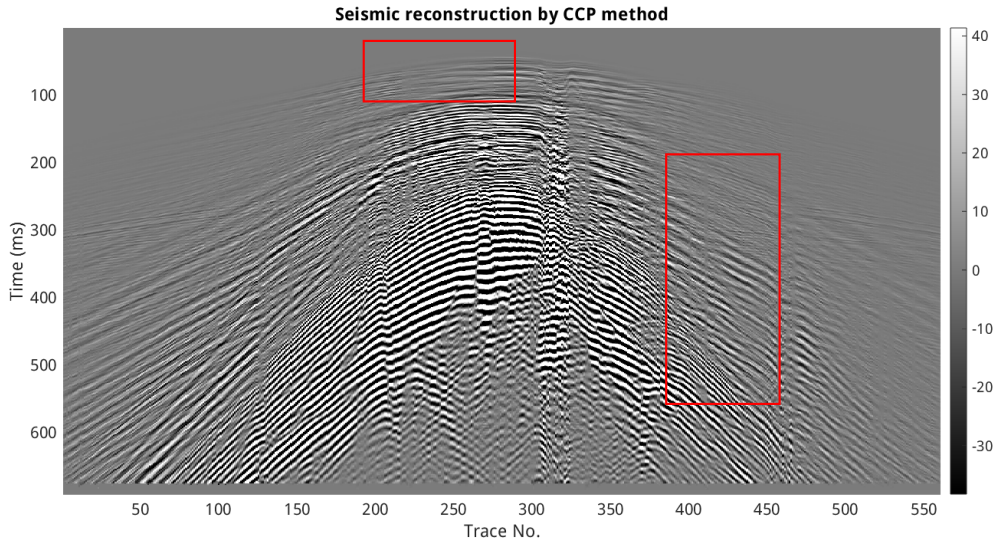

(b)

Figure 3-10: The reconstructed 2D seismic section NO. 200 using **(a)** the CP method and **(b)** the CCP method.

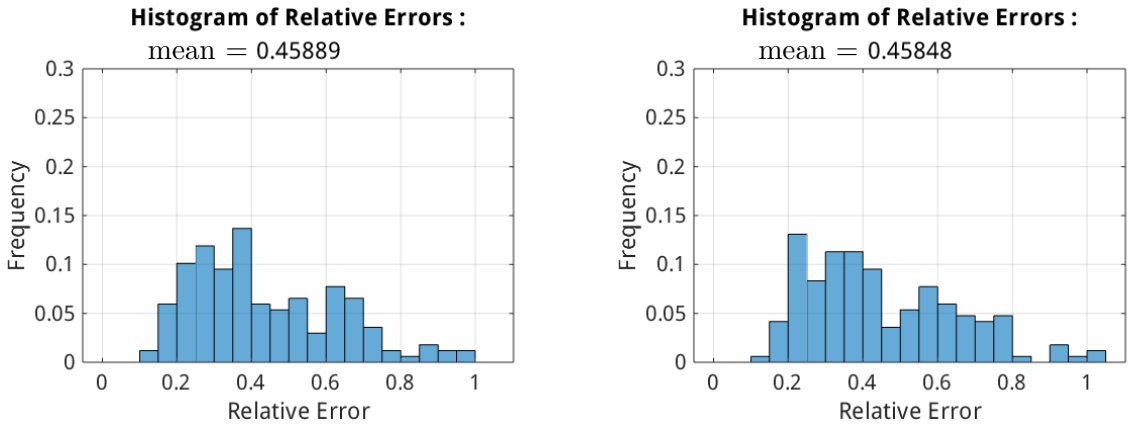

Figure 3-11: Histogram of the metric function for **(a)** Figure 3-10a and **(b)** 3-10b.

3-5 3D seismic model cube reconstruction

3-5-1 Local traveltime operators in NLBF

Nonlinear Beamforming (NLBF) is a recently proposed technology aimed at enhancing the quality of raw seismic data obtained through modern data acquisition schemes.[2]. NLBF works in two stages: initially, it estimates local kinematic wavefronts within the input data, then, perform a weighted summation for each trace in the input data with its neighboring traces along the identified local kinematic wavefronts.

NLBF employs local traveltime operators as mathematical tools to describe local kinematic wavefronts.[2] In NLBF, local traveltime operators are described by a second-order equation:

$$\Delta t(x,y;x_0,y_0) = A(x-x_0)+B(y-y_0)+C(x-x_0)(y-y_0)+D(x-x_0)^2+E(y-y_0)^2, \quad (3\text{-}2)$$

where (x_0, y_0) is the NLBF parameter trace location, (x, y) is the trace location in the input seismic data, and A, B, C, D, E are the five parameters that need to be obtained by maximizing the semblance-based cost function[24]:

$$S(x_0,y_0) = \frac{\sum_{j=1}^{N}\{\sum_{i=1}^{M} u[x_i,y_i;t_j(x_0,y_0)+\Delta t(x,y;x_0,y_0)]\}^2}{M\sum_{j=1}^{N}\sum_{i=1}^{M}\{u[x_i,y_i;t_j(x_0,y_0)+\Delta t(x,y;x_0,y_0)]\}^2}, \quad (3\text{-}3)$$

where $u(x_i, y_i; t)$ is a time sample of the traced located at (x_i, y_i). M is the number of traces in the spatial aperture and N is the number of time samples in the temporal aperture of a local traveltime operators. The NLBF parameter cubes calculated by the 2+2+1 method on a SEAM Arid dataset[17][23] are our reference results. 30% of the NLBF parameter traces are randomly decimated to form the sparse input for the CCP method to reconstruct.

3-5-2 Results

The reconstruction results of the 3D seismic model cube using the CP and CCP methods are shown in Figures 3-12 to 3-16. The 3D seismic model cubes are with the dimension of 690*41*40 data points. Both the CP and the CCP method use a 3D reconstruction window of 64*41*40 data points, and the window moving step is 16 points in the first direction. Specifically, Figures 3-12a, 3-13a, 3-14a, 3-15a and 3-15a present the reference result of parameters A, B, C, D, and E, respectively. Figures 3-12b, 3-13b, 3-14b, 3-15b, and 3-16b are the sparse input with 30% randomly decimated parameter traces. It is important to note that the data sets shown in Figure 3-12a to Figure 3-16a serve merely as references rather than the ground truth due to how NLBF parameters are estimated. Consequently, we do not use our metric function to evaluate the reconstruction quality in this example. However, by directly observing the results of CP and CCP reconstruction, we can see that the ringing noise has been suppressed in the highlighted areas in Figure 3-12c, 3-12d, 3-13c, 3-13d, 3-14c, 3-14d, 3-15c, 3-15d, 3-16c, 3-16d.

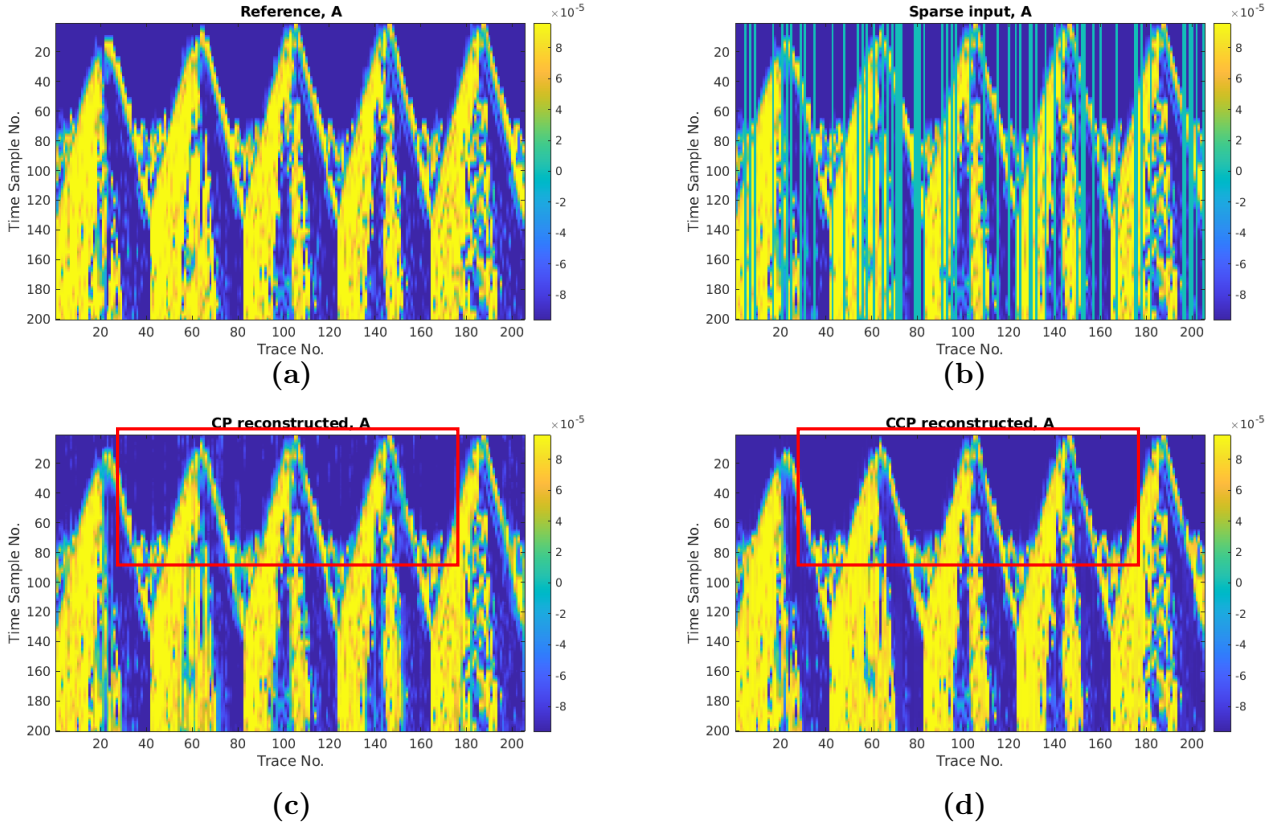

Figure 3-12: **(a)** NLBF reference of parameter A. **(b)** Sparse input A cube with 30% randomly decimated NLBF parameter traces **(c)** Reconstructed A by CCP. **(d)** Reconstructed A by CP. The red box highlights that part shows the ringing noise is suppressed.

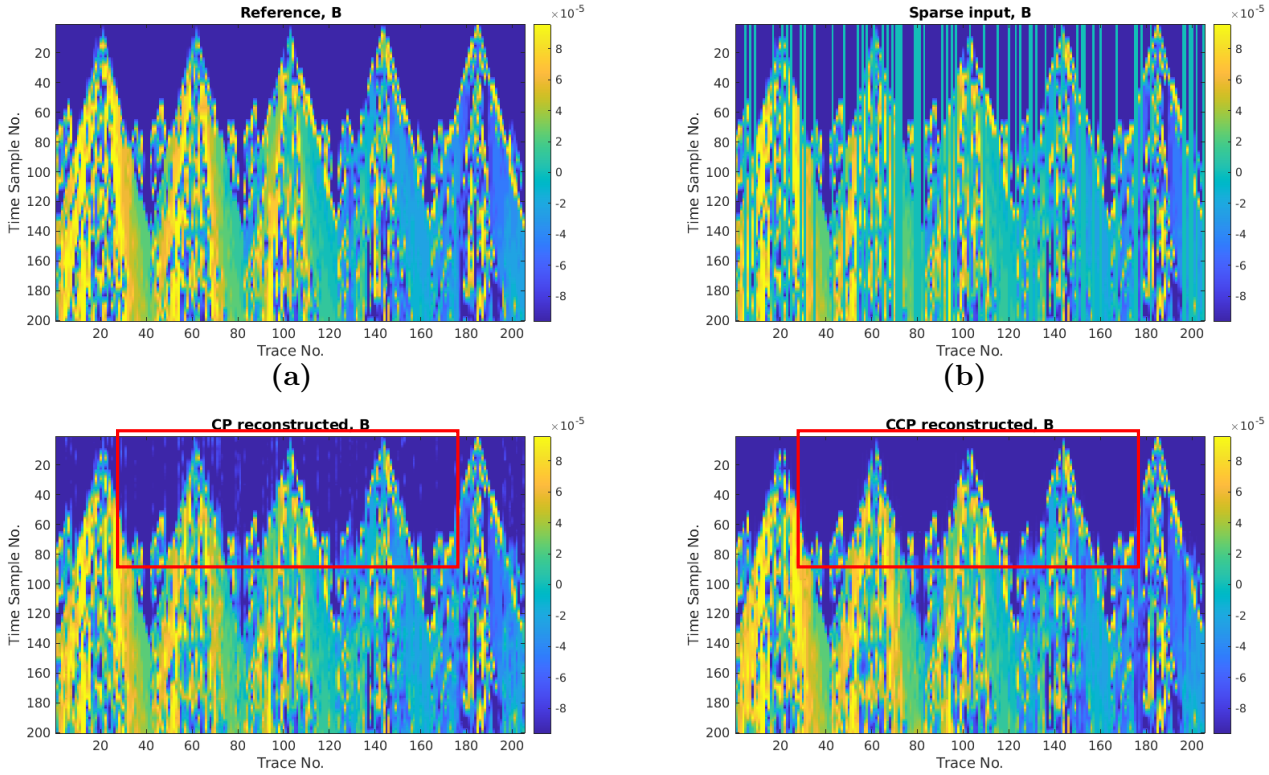

Figure 3-13: **(a)** NLBF reference of reference B. **(b)** Sparse input B cube with 30% randomly decimated NLBF parameter traces **(c)** Reconstructed B by CCP. **(d)** Reconstructed B by CP. The red box highlights that the ringing noise is suppressed.

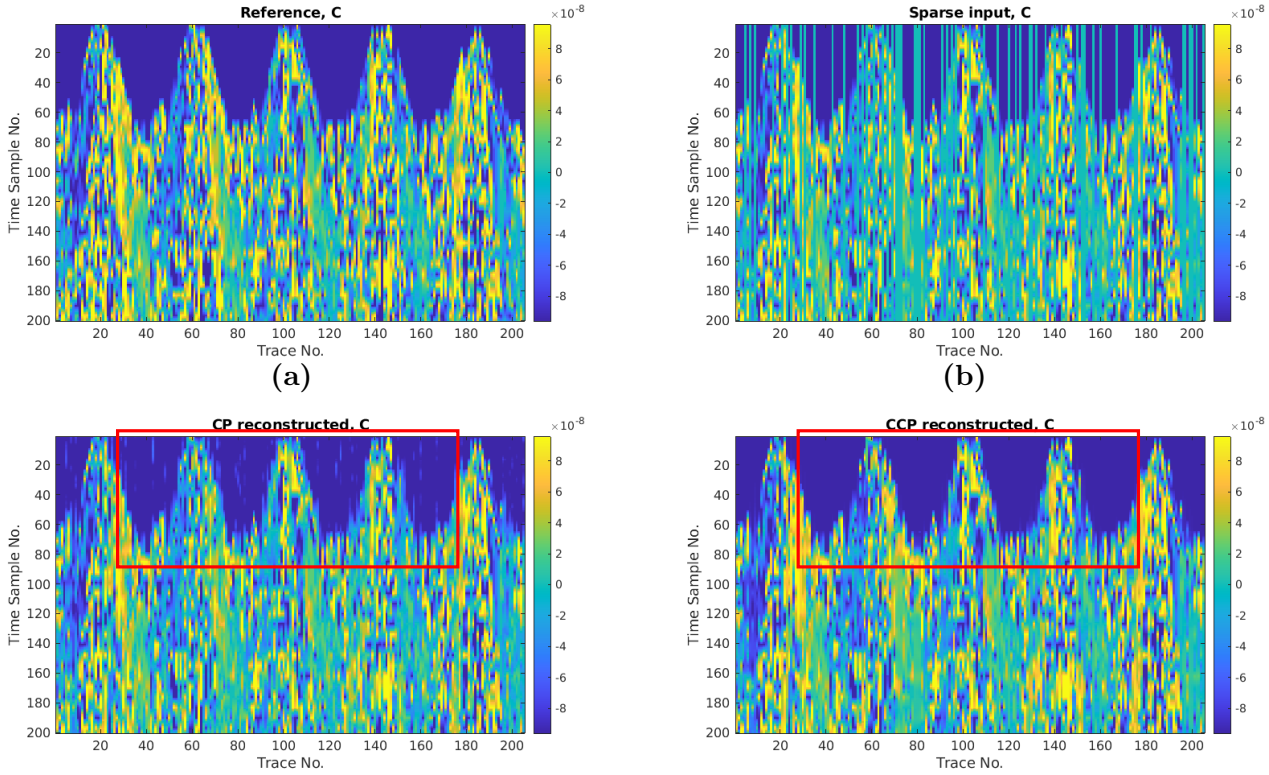

Figure 3-14: **(a)** NLBF reference of parameter C. **(b)** Sparse input C cube with 30% randomly decimated NLBF parameter traces **(c)** Reconstructed C by CCP. **(d)** Reconstructed C by CP. The red box highlights that the ringing noise is suppressed.

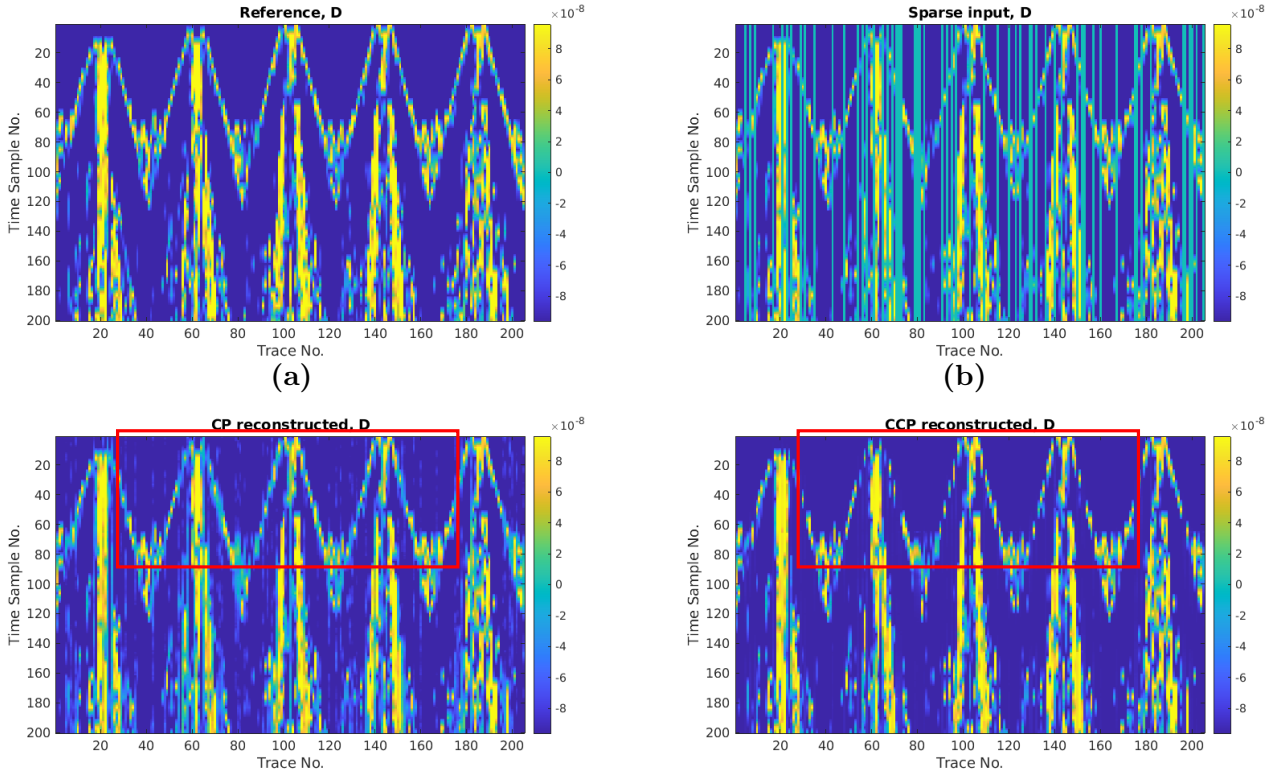

Figure 3-15: **(a)** NLBF reference of parameter D. **(b)** Sparse input D cube with 30% randomly decimated NLBF parameter traces **(c)** Reconstructed D by CCP. **(d)** Reconstructed D by CP. The red box highlights that the ringing noise is suppressed.

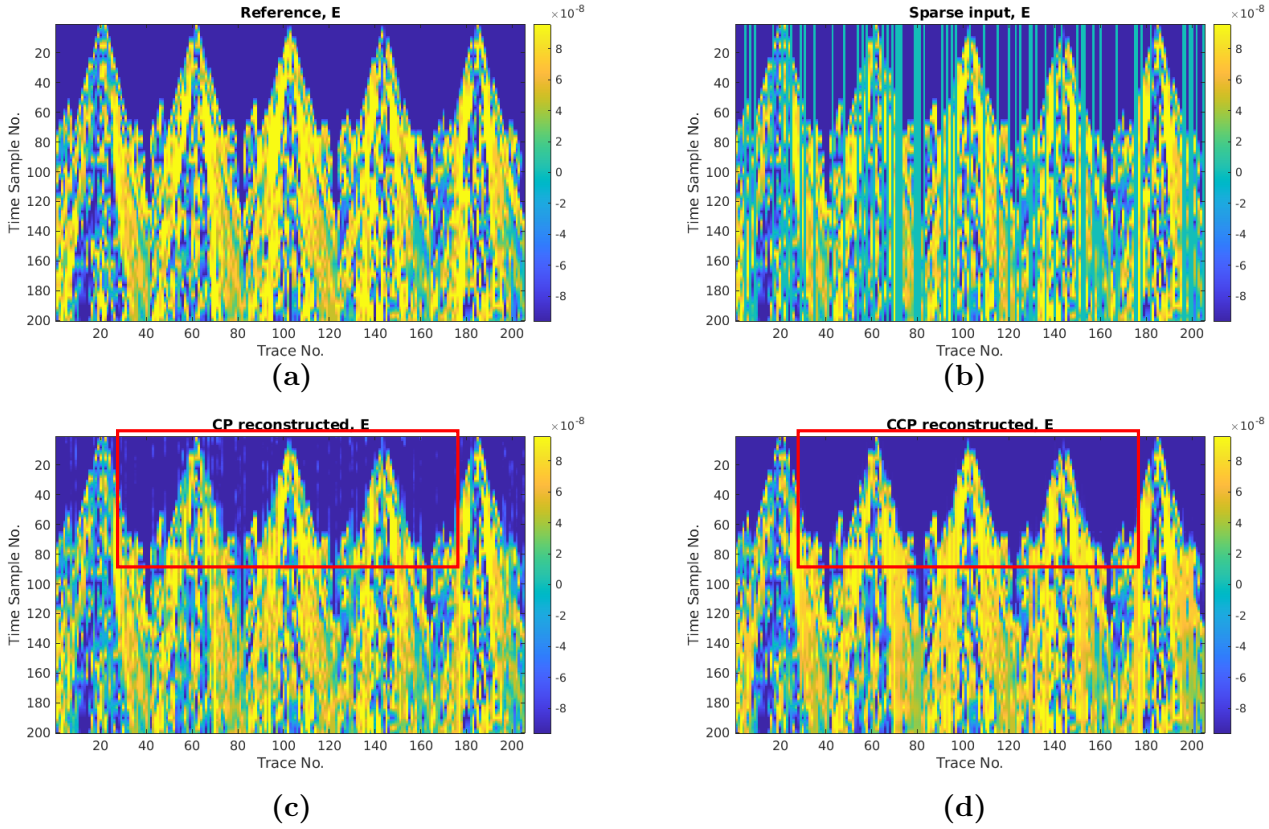

Figure 3-16: **(a)** NLBF reference of parameter E. **(b)** Sparse input E cube with 30% randomly decimated NLBF parameter traces **(c)** Reconstructed E by CCP. **(d)** Reconstructed E by CP. The red box highlights that the ringing noise is suppressed.

The reconstruction results from the three examples above all indicate that, compared to the CP method, the CCP method can suppress the ringing noise and greatly improve the reconstruction quality. For the reconstructed results in images the CCP method's reconstruction results are sharper and clearer. For the reconstruction results of 2D seismic sections and 3D seismic model cubes, the ringing noise in areas where seismic waves have not reached is reduced.

Chapter 4

Discussion

In this chapter, we reveal some in-depth insights when using the CCP method for data reconstruction. We delve into the CCP reconstruction loop, using a 2D seismic data slice as an example, to observe the result evolution during the whole CCP process. Additionally, we compare the results of applying the CCP non-local means algorithm to the CP reconstructed results with the results of the CCP method, justifying the value of the CCP method. We also demonstrate the value of the data preconditioning in our current CCP method. Finally, we conduct parameter testing and propose a set of empirical control parameters for the CCP method.

4-1 Intermediate results in the outer loop of the CCP method

In chapter 3, the maximum iteration number N used in the CCP method is 10. We hereby use one reconstruction window in Figure 4-1 to illustrate all the intermediate results in the outer loop of the CCP method, demonstrating the result evolution process. All the control parameters are the same as in chapter 3. Figure 4-1 shows the CCP reconstructed results after different times outer loop iteration numbers. Figure 4-1a is the ground truth of a 2D section shot gather. Figure 4-1 is the sparse input with 30% randomly decimated traces. Figures 4-1c to 4-1m demonstrate how the CCP non-local means algorithm tweaks the initial value after every outer loop iteration.

Figure 4-2a illustrates the reconstructed result using the CP method within the selected window. Figure 4-2b presents the reconstructed result obtained by the CCP method after all the outer loops. The red boxes highlight the presence of ringing noise in the reconstructed results. Notably, the ringing noise in the CCP method's reconstructed result was significantly suppressed, demonstrating the effectiveness of our idea in adjusting the initial values during the outer loop.

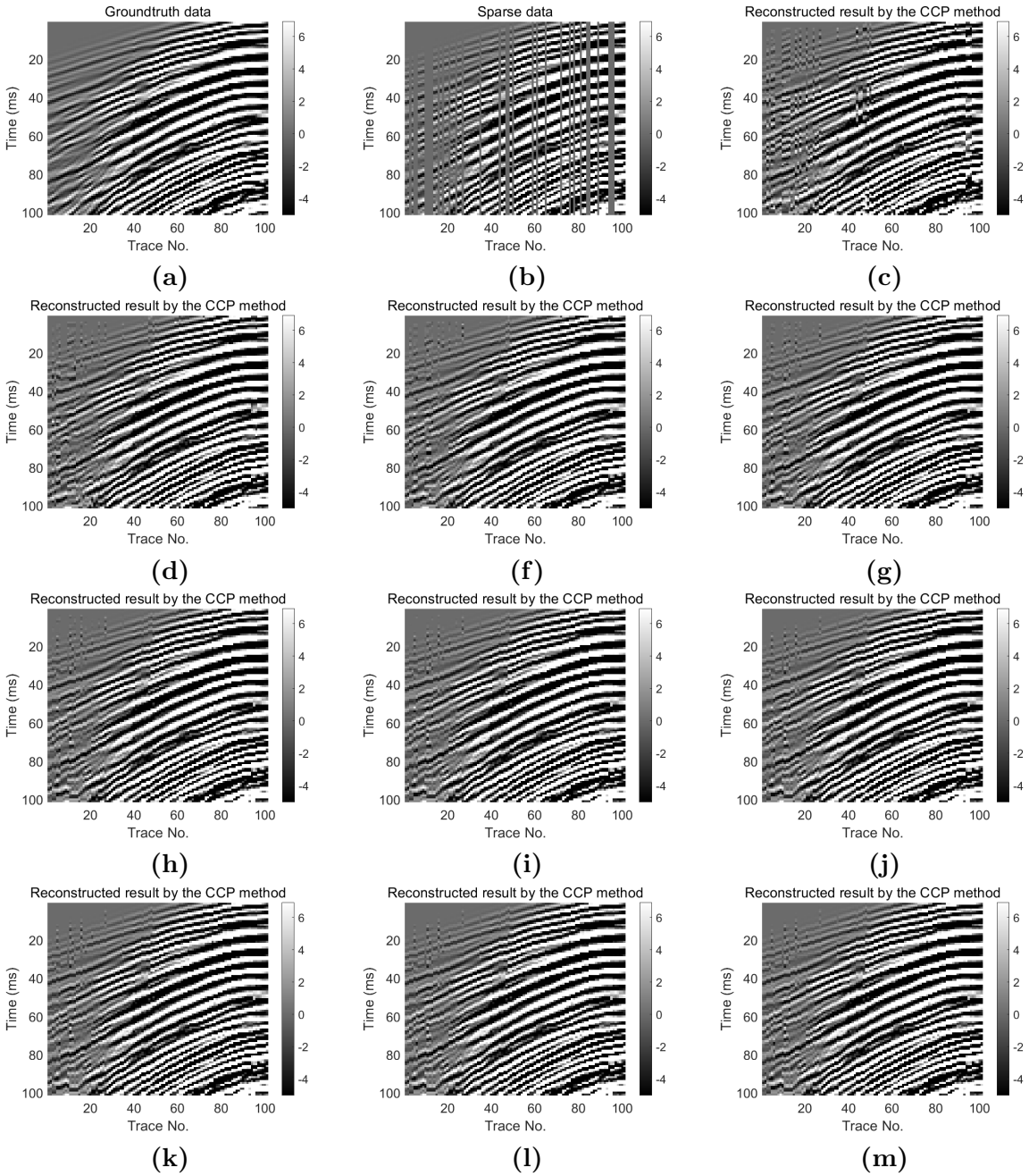

Figure 4-1: **(a)** Ground truth of a 2D section shot gather. **(b)** Sparse data with 30% randomly decimated traces. **(c)-(m)** Intermediate results in the 1st to 10th outer loop of the CCP method.

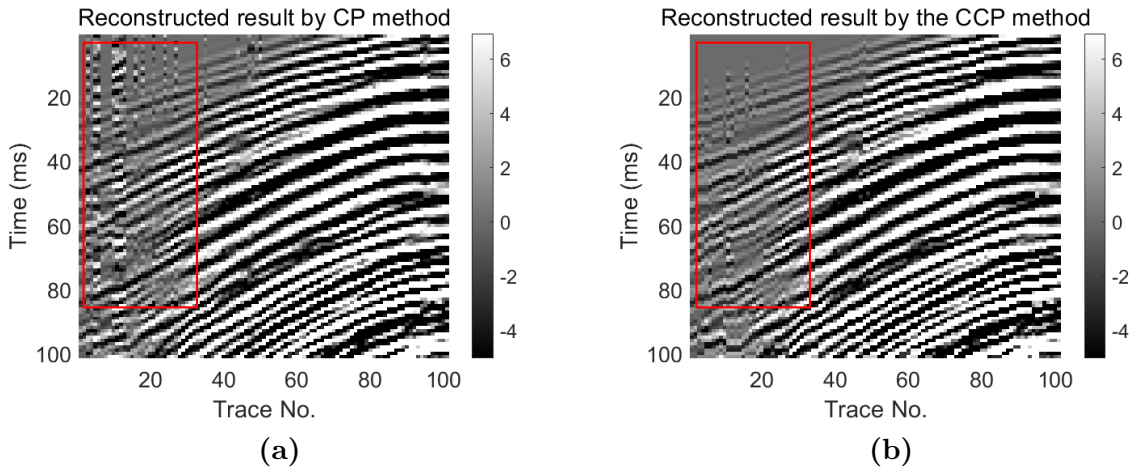

(a) (b)

Figure 4-2: **(a)** Reconstructed result of Figure4-1b by the CP method. **(b)** Reconstructed final result of Figure4-1b by the CCP method.

4-2 CCP non-local means algorithm on the CP method

We compare the results of applying the CCP non-local means algorithm after CP reconstruction with the results of the CCP method only in Figure 4-3. Figure 4-3a is the ground truth of a 2D section shot gather. Figure 4-3 is the sparse input with 30% decimated traces. Figure 4-3c is the reconstruction result by the CP method with one time CCP non-local means algorithm. Figure 4-3d is the reconstructed result by the CCP method. Figure 4-3e and 4-3f are the corresponding metric function's histogram with mean value of Figure 4-3c and 4-3d. The Figure 4-3c indicates that the CCP non-local means algorithm can suppress ringing noise to a CP reconstructed result. Moreover, incorporating the CCP non-local means algorithm as a step for tweaking the initial values in the CCP method can further reduce ringing noise in the reconstructed result as it shown in Figure 4-3d.

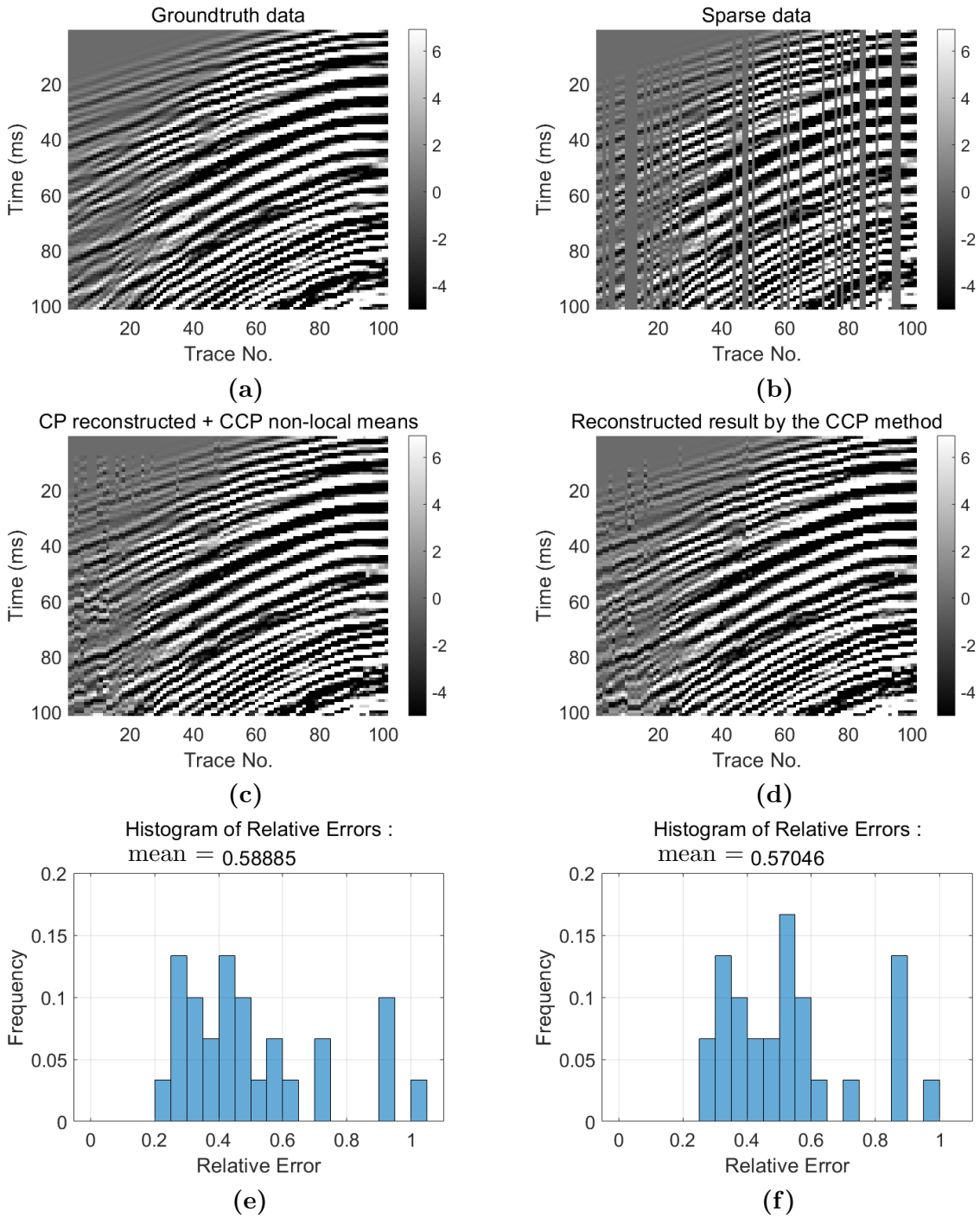

Figure 4-3: **(a)** Ground truth of a 2D section shot gather. **(b)** Sparse data with 30% randomly decimated traces. **(c)** Reconstructed result by implemented CCP non-local means into the CP reconstructed result. **(d)** Reconstructed result of the CCP method. **(e)** Metric function of Figure 4-3c. **(f)** Metric function of Figure 4-3d.

4-3 Data preconditioning

The optional preconditioning step is used to address the issue of excessively large or small dynamic ranges in the input data being processed as we mentioned in chapter2. Here we present an example to demonstrate the improvement of the final result through the preconditioning step.

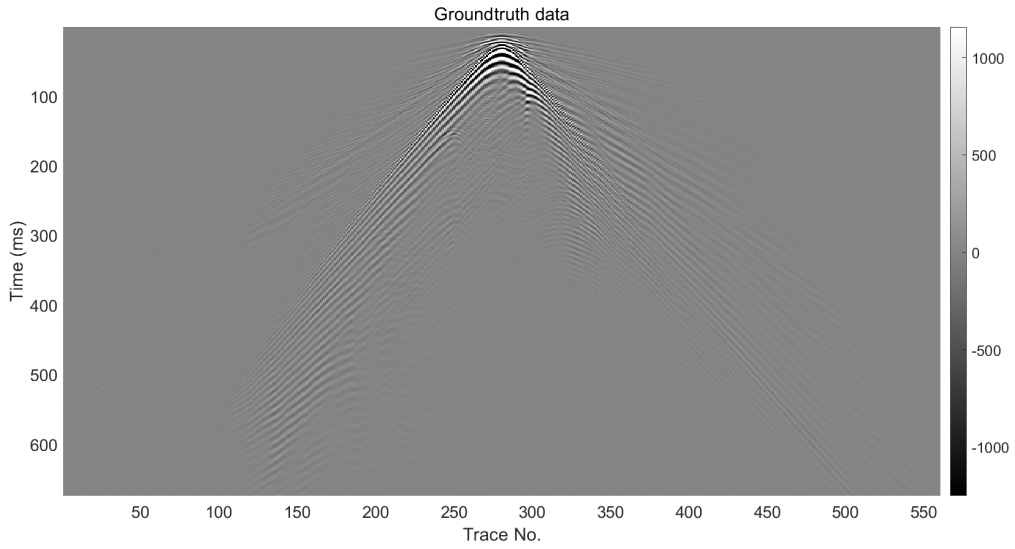

(a)

(b)

Figure 4-4: **(a)** Ground truth of the 2D section NO. 270 **(b)** Sparse input with 30% randomly decimated traces.

Figures 4-4 through 4-5 illustrate the comparison of results for data with a large dynamic range, with and without the use of preconditioning. Figure 4-5a is the reconstructed result

by the CCP method without preconditioning. Figure 4-5b is the reconstructed result by the CCP method with preconditioning. Without preconditioning, an excessively large dynamic range may cause the CCP non-local means algorithm to calculate weights between different patches too small, resulting in some weights being ignored. The red highlighted areas show how this large dynamic range influence the reconstruction results.

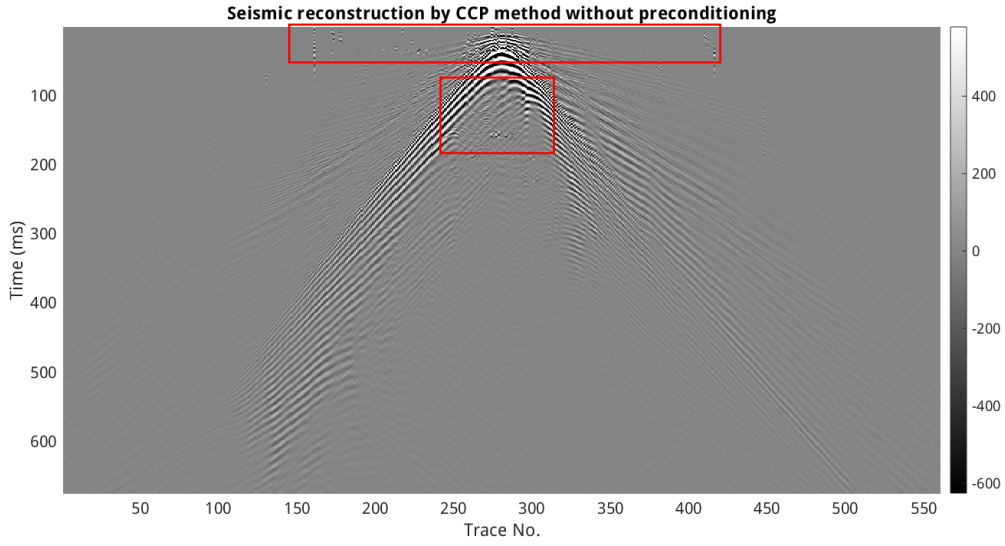

(a)

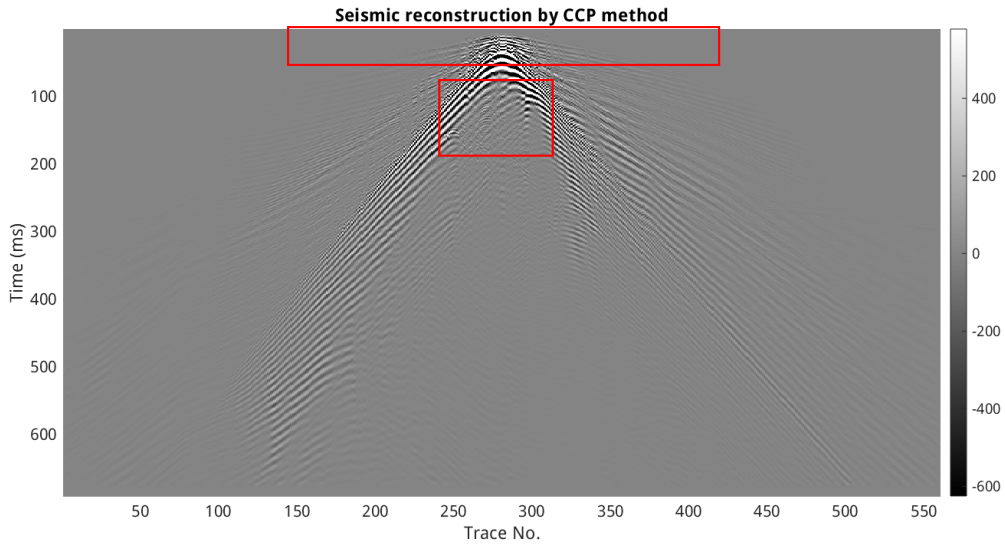

(b)

Figure 4-5: **(a)** CCP reconstructed result of the 2D section NO. 270 **(b)** CCP reconstructed result of the 2D section NO. 270 without preconditioning.

4-4 Parameter testing

Four control parameters exist in our CCP non-local means algorithm, including the reference patch size, the search window size, the filter sigma h, and the Gaussian kernel ratio α in equations (2-1) through (2-3). We carry out parameter testing using several input data to gain an empirical understanding on how to set their values in realistic applications.

We test all the control parameters in the CCP method based on the common control parameters: maximum iteration number N is 10, convergence ratio ϵ is 0.01, and the thresholding function is defined in equations (1-21) to (1-23). Due to the large computational workload, we are unable to conduct global parameter testing across four dimensions. Instead, we adopted the following strategy for local parameter testing:

1. Set four initial control parameters for the CCP reconstruction.
2. Test control parameter 1 based on the three initial control parameters to find the best parameter 1.
3. Update to the best control parameter 1.
4. Test control parameter 2 based on the two initial control parameters and the best control parameter 1.
5. Based on the previous steps, update the best control parameters 2, 3, and 4.

First, we use the above method to test the CCP parameters for 2D seismic data reconstruction, section NO.270 and NO.200. Here a reconstruction window of 128 pixels by 128 pixels, and the window moving step is 16 in both directions. The parameters 1, 2, 3, and 4 correspond to patch size, the search window size, the Gaussian kernel ratio α, and filter sigma h, respectively. We set the initial window size to 21, alpha to 0.3, and filter sigma h to 0.1. The patch size is set within the range [3, 5, 7, 9, 11, 13, 15]. We select the patch size value (patch size is 15) corresponding to the minimum mean statistical error in the results as the best testing result. The results are shown in Figure 4-6a and Figure 4-7a. The search window size is set within the range [7, 11, 15, 19, 23, 27, 31]. It is important to note that the first two values in this range are smaller than the best patch size updated. Since the search window size should not be lower than the patch size, the first two calculations for parameter testing of the search window size are skipped. The results are shown in Figure 4-6b and Figure 4-7b. We continue with parameter testing for Gaussian kernel ratio α and filter sigma h within range [0.05, 0.10, 0.15, 0.20, 0.25, 0.30, 0.35, 0.40, 0.45, 0.50] in the same manner. The results are shown in Figures 4-6c 4-6d 4-7c and 4-7d. Ultimately, we obtained a set of empirical parameters of the CCP method for 2D seismic data reconstruction: the patch size is 15 the search window size is 19, the Gaussian kernel ratio α is 0.30 and the filter sigma h is 0.10.

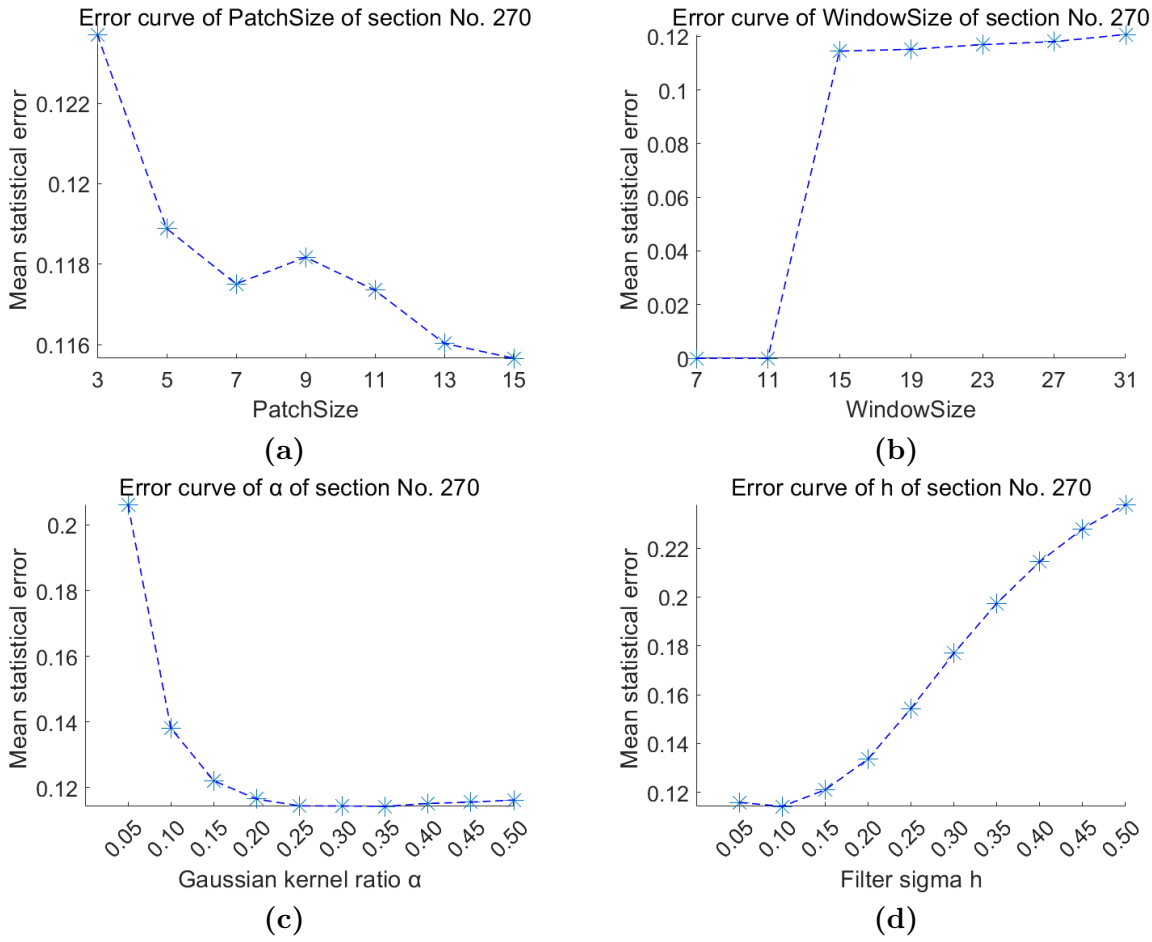

Figure 4-6: Parameter testing result of seismic section NO. 270 reconstrution **(a)** Error curve of PatchSize. **(b)** Error curve of WindowSize. **(c)** Error curve of α. **(d)** Error curve of h.

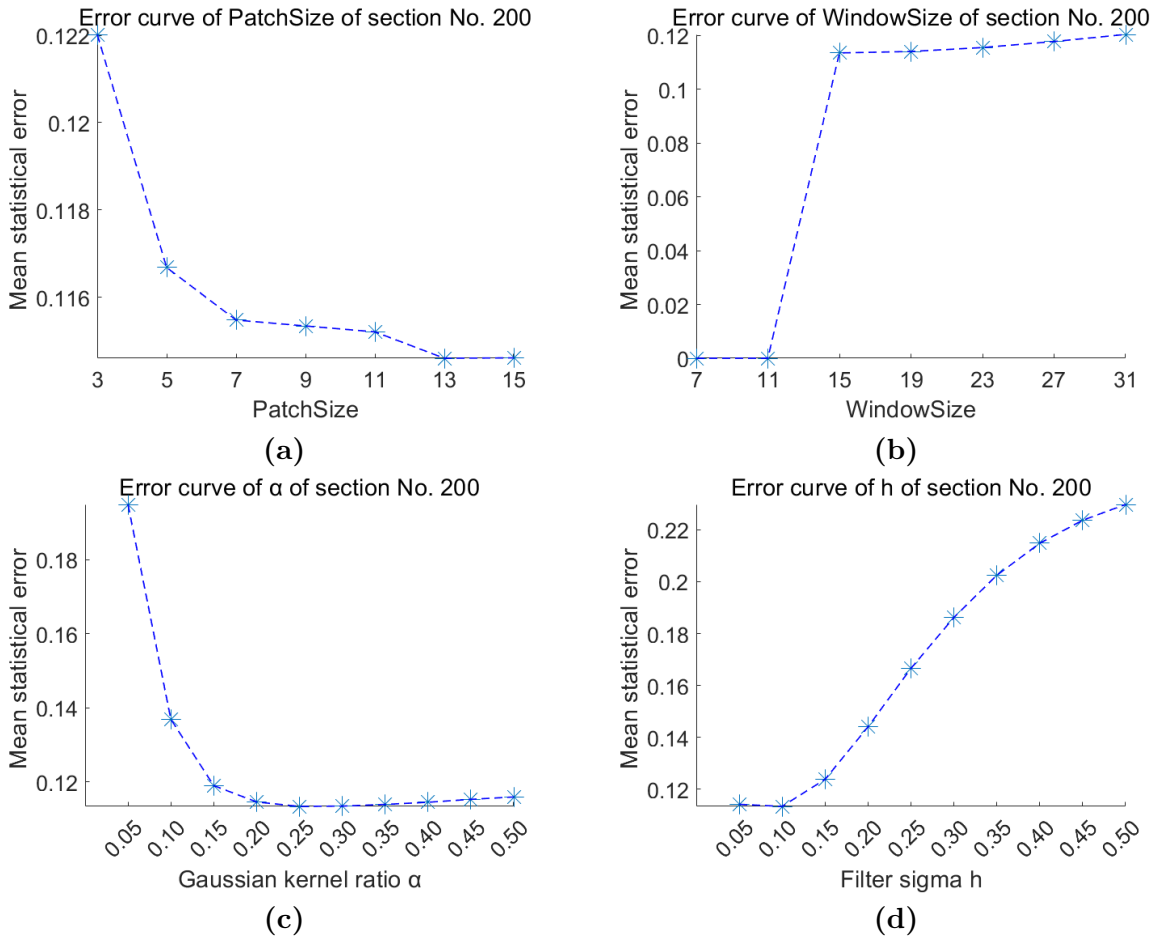

Figure 4-7: Parameter testing result of seismic section NO. 200 reconstruction **(a)** Error curve of PatchSize. **(b)** Error curve of WindowSize. **(c)** Error curve of α. **(d)** Error curve of h.

Then, we use the above method to test the CCP parameters for image reconstruction (the Mars desert image and the drill cuttings image used in chapter3). Here a reconstruction window of 128 pixels by 128 pixels, and the window moving step is 64 in both directions. The parameters 1, 2, 3, and 4 correspond to patch size, the search window size, the Gaussian kernel ratio α, and filter sigma h, respectively. We set the initial window size to 21, alpha to 4, and filter sigma h to 10. The patch size is set within the range [3, 5, 7, 9, 11, 13, 15]. We select the patch size value (patch size is 5) corresponding to the minimum mean statistical error in the results as the best testing result. The results are shown in Figure 4-8a and Figure 4-9a. The search window size is set within the range [7, 11, 15, 19, 23, 27, 31]. The results are shown in Figure 4-8b and Figure 4-9b. We continue with parameter testing for Gaussian kernel ratio α within the range 1-10 and filter sigma h within the range 0-90 in the same manner. The results are shown in Figures 4-8c 4-8d 4-9c and 4-9d. Ultimately, we obtained a set of empirical parameters of the CCP method for image reconstruction: the patch size is 5 the search window size is 7-15, the Gaussian kernel ratio α is 3 and the filter sigma h is 10.

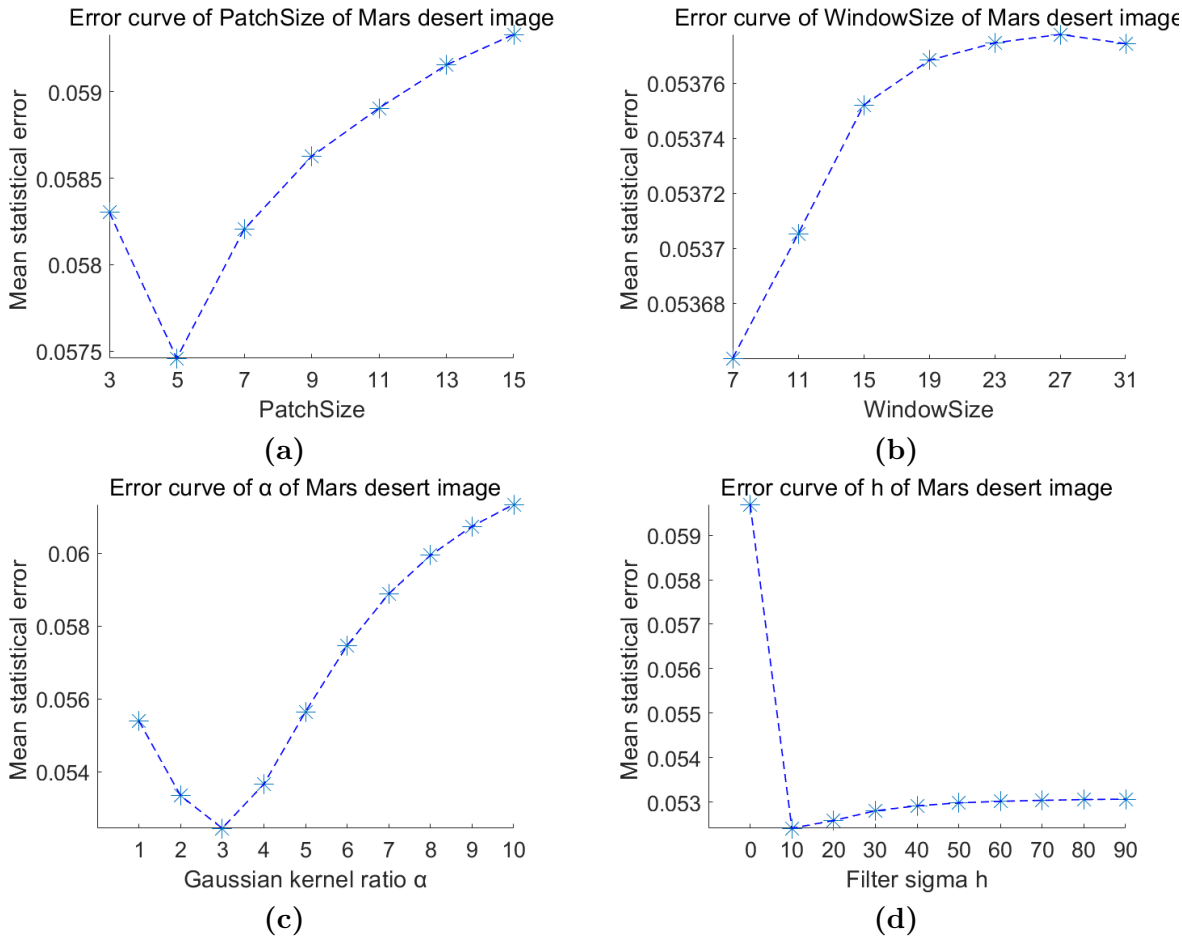

Figure 4-8: Parameter testing result of Mars desert image reconstruction **(a)** Error curve of PatchSize. **(b)** Error curve of WindowSize. **(c)** Error curve of α. **(d)** Error curve of h.

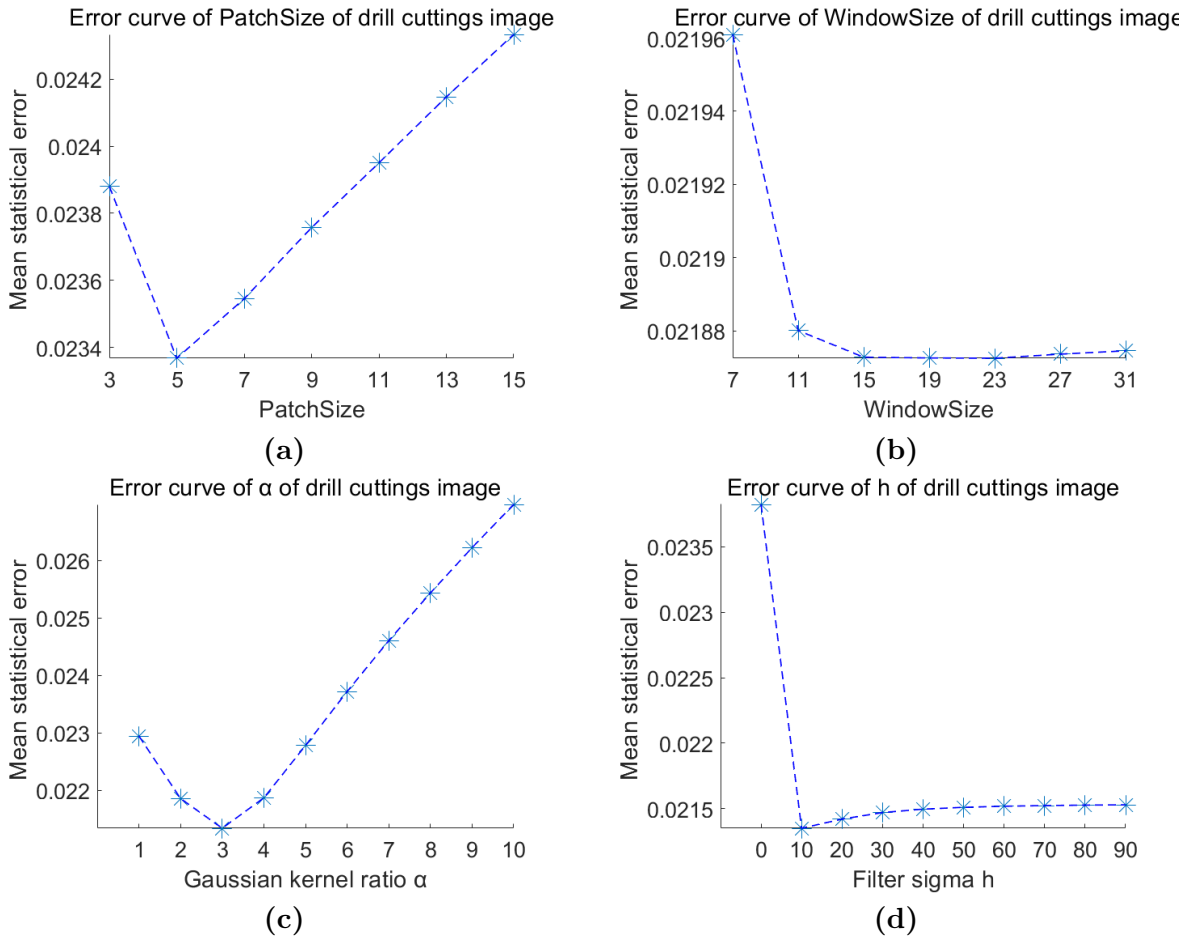

Figure 4-9: Parameter testing result of drill cuttings image reconstruction **(a)** Error curve of PatchSize. **(b)** Error curve of WindowSize. **(c)** Error curve of α. **(d)** Error curve of h.

We present a set of empirical parameters in table 4-1 for different data types in the CCP method. Due to computational limitations, we have temporarily postponed parameter testing for the reconstruction of the 3D seismic model. However, we still provide the empirically determined parameters that yielded good results for this project.

Table 4-1: Default control parameters of the CCP method for different data.

Data	Patch Size	Window Size	α	h
Image Data	5	11	3	10
2D Seismic	15	19	0.30	0.10
3D Model	5	9	0.20	0.10

Chapter 5

Conclusions

In this thesis, we have discussed the theory and methodology of the CCP method. Our goal is to improve the existing CP method framework into the CCP method, so that the ringing noise in the reconstructed results is suppressed. We utilized different types of data for the CCP method reconstruction, including images, 2D seismic data, and 3D seismic model cubes and comparing the CCP reconstructed results with the CP reconstructed result. Our aim is to address the research question: can the CCP method suppress the ringing noise in the reconstructed results comparing with the CP reconstructed results? Our conclusions are as follows:

- The concept of the CCP method is to tweak the values after projection during the alternating projections of the CP method, guiding them towards a desired direction. This new projection result provides a more preferable solution to the under-determined reconstruction problem. To achieve this, we designed the CCP non-local means algorithm, based on the non-local means algorithm, to suppress the ringing noise caused by the hard thresholding function in the CP method.

- Similar to the CP method, the CCP method can reconstruct various types of data, including photographic images, 2D seismic data sections, and 3D seismic model cubes. In Chapter 3 we present the reconstruction results using the CCP method. We use the relative error between each reconstructed element and the corresponding element in the ground truth as our quality metric function. The results of reconstructing different types of data using the CCP method show less ringing noise and higher quality compared to the CP method, both when evaluated by the quality metric function and through direct observation.

- We gain in-depth insights into the use of the CCP method for data reconstruction. By examining the CCP reconstruction loop with a 2D seismic data slice, we observe the evolution of the results throughout the entire CCP process. We compare the outcomes of applying the CCP non-local means algorithm to the CP reconstructed results with those obtained directly from the CCP method, demonstrating that the results from

the CCP method are better. Furthermore, we demonstrated the importance of data preconditioning in the current CCP method. Lastly, we conducted parameter testing and proposed a set of empirical control parameters for optimizing the CCP method.

- Overall, the application of the CCP method for data reconstruction represents a novel approach. The scope of our research was limited by the timeframe of the IDEA League Applied Geophysics Master's thesis. There are two additional research directions to further explore: 1) employing tweaking methods other than the CCP non-local means algorithm for initial values tweaking, and 2) while this study primarily focused on the outer loop of the CCP method, specifically tweaking the initial values in the data domain, initial values tweaking could also be applied in the $f - k_x$ domain.

Bibliography

[1] R. Abma and M.N. Kabir. 3d interpolation of irregular data with a pocs algorithm. *Geophysics*, 71(6):E91–E97, 2006.

[2] A. Bakulin, I. Silvestrov, M. Dmitriev, D. Neklyudov, M. Protasov, K. Gadylshin, and V. Dolgov. Nonlinear beamforming for enhancement of 3d prestack land seismic data. *Geophysics*, 85(3):V283–V296, 2020.

[3] L.M. Bregman. Finding the common point of convex sets by the method of successive projection. *Comput. Math. Math. Phys.*, 162(3):487–490, 1965.

[4] A. Buades, B. Coll, and J.M. Morel. A non-local algorithm for image denoising. In *2005 IEEE Computer Society Conference on Computer Vision and Pattern Recognition*, volume 2, pages 60–65 vol. 2, 2005.

[5] Y. Chen, J. Ma, Q. Feng, L. Luo, P. Shi, and W. Chen. Nonlocal prior bayesian tomographic reconstruction. *Journal of Mathematical Imaging and Vision*, 30:133–146, 2008.

[6] J.J. Gao, X.H. Chen, J.Y. Li, G.C. Liu, and J. Ma. Irregular seismic data reconstruction based on exponential threshold model of pocs method. *Applied Geophysics*, 7:229–238, 2010.

[7] R.W. Gerchberg. Super-resolution through error energy reduction. *Optica Acta: International Journal of Optics*, 21(9):709–720, 1974.

[8] L.G. Gubin, B.T. Polyak, and E.V. Raik. The method of projections for finding the common point of convex sets. *USSR Computational Mathematics and Mathematical Physics*, 7(6):1–24, 1967.

[9] G. Hennenfent, L. Fenelon, and F.J. Herrmann. Nonequispaced curvelet transform for seismic data reconstruction: A sparsity-promoting approach. *Geophysics*, 75(6):WB203–WB210, 2010.

[10] A.O. Hero and D. Blatt. Sensor network source localization via projection onto convex sets (pocs). *Proceedings. (ICASSP '05). IEEE International Conference on Acoustics, Speech, and Signal Processing, 2005.*, pages iii/689–iii/692 Vol. 3, 2005.

[11] Q. Hirsch. Nonlinear beamforming seismic data reconstruction: A novel kinematic wavefront based method. *MSc thesis, TU Delft*, 2022.

[12] J. Huang, J. Ma, N. Liu, H. Zhang, Z. Bian, Y. Feng, Q. Feng, and W. Chen. Sparse angular ct reconstruction using non-local means based iterative-correction pocs. *Computers in Biology and Medicine*, 41(4):195–205, 2011.

[13] P.A. Jansson and R.J. Marks. *Deconvolution of Images and Spectra: Chapter14. Alternating Projectionsonto Convex Sets.* Dover Publications, 2014.

[14] M.M.N. Kabir and D.J. Verschuur. Restoration of missing offsets by parabolic radon transform. *Geophysical Prospecting*, 43(3):347–368, 1995.

[15] J. Ma, Q. Feng, Y. Feng, J. Huang, and W. Chen. Generalized gibbs priors based positron emission tomography reconstruction. *Computers in biology and medicine*, 40(6):565–571, 2010.

[16] R.J. Marks and D.K. Smith. Gerchberg-type linear deconvolution and extrapolation algorithms. In *Transformations in Optical Signal Processing*, volume 373, pages 161–178. SPIE, 1984.

[17] M. Oristaglio. Seam update. *The Leading Edge*, 35(10):912–915, 2016.

[18] A. Papoulis. A new method of image restoration. *JSTAC, Paper VI-3*, 1973.

[19] M.I. Sezan and H. Stark. Image restoration by the method of convex projections: Part 2-applications and numerical results. *IEEE Transactions on Medical Imaging*, 1(2):95–101, 1982.

[20] M.I. Sezan, H. Stark, and S.J. Yeh. Projection method formulations of hopfield-type associative memory neural networks. *Appl. Opt.*, 29(17):2616–2622, Jun 1990.

[21] A. Stanton, M. Sacchi, R. Abma, and J. Stein. Mitigating artifacts in projection onto convex sets interpolation. All Days:SEG–2015–5754691, 2015.

[22] Y. Sun and Q. Hirsch. A convergent alternating projections onto convex sets method for data reconstruction. *Geophysics*, 89(1):V49–V63, 2024.

[23] Y. Sun, I. Silvestrov, and A. Bakulin. Accelerating the 2+2+1 method for estimating local traveltime operators in nonlinear beamforming using gpu graphics cards. *Journal of Geophysics and Engineering*, 19(3):389–402, 06 2022.

[24] Y. Sun, I. Silvestrov, and A. Bakulin. Enhancing 3-d land seismic data using nonlinear beamforming based on the efficiency-improved genetic algorithm. *IEEE Transactions on Evolutionary Computation*, 26(5):1192–1199, 2022.

[25] Z. Sylvester. https://github.com/zsylvester/segmenteverygrain/commit/5245f82ebda5052be2feed25482699b5cead3c65, 2024.07.07.

[26] D.C. Youla and H. Webb. Image restoration by the method of convex projections: Part 1: Theory. *IEEE Transactions on Medical Imaging*, 1(2):81–94, 1982.